Complexome profile of mitochondrial complexes in the myzozoan parasite of oysters, *Perkinsus marinus*

Andrew E. Maclean[1,2,3]*, Orsola Iorillo[4,5], Drahomíra Faktorová[4,5], Monika Singh[2,3], Suzanne McGill[6], Julius Lukeš[4,5,*], Lilach Sheiner[2,3,*]

[1]Institute for Immunology and Infection Research, University of Edinburgh, Edinburgh, United Kingdom
[2]Centre for Parasitology, University of Glasgow, Glasgow, United Kingdom
[3]School of Infection and Immunity, University of Glasgow, Glasgow, United Kingdom
[4] Institute of Parasitology, Biology Centre, Czech Academy of Sciences, České Budějovice, Czech Republic
[5]Faculty of Science, University of South Bohemia, České Budějovice, Czech Republic
[6] College of Medical, Veterinary & Life Sciences Shared Research Facilities, University of Glasgow, Glasgow, United Kingdom

*Joint corresponding authors

For correspondence: andrew.maclean@ed.ac.uk; jula@paru.cas.cz; Lilach.sheiner@glasgow.ac.uk

Abstract

Mitochondrial complexes, such as the mitochondrial electron transport chain (mETC), the F_1F_o-ATP synthase and the mitochondrial ribosome, are centrally important for mitochondrial function. Recently, an unexpected diversity in the composition of these complexes across unicellular eukaryotic lineages, with the apicomplexan parasites featuring prominently, has been revealed. However, whether the observed enlarged and divergent mitochondrial complexes are conserved across the wider Myzozoan lineage has not been investigated. Here, using a complexome profiling proteomic approach, we have characterised the composition of the mitochondrial complexes of the myzozoan parasite of oysters, *Perkinsus marinus*. We show that it shares with *Plasmodium* and *Toxoplasma* huge ATP synthase and mETC complexes. Moreover, the *Perkinsus* mitoribosome possesses many of the divergent features recently discovered in apicomplexans, such as an expanded subunit repertoire and the inclusion of RAP-domain and ApiAP2-like proteins as ribosomal proteins. Our study reveals the divergent subunit composition of mitochondrial complexes is an ancestral and highly conserved feature of Myzozoa.

Introduction

Mitochondria are double membrane bound organelles which are a unique feature of eukaryotes and, despite reduction or loss in some lineages, play an ever-increasing number of vital roles in their biology, ranging from energy metabolism to biosynthesis of key metabolites [1]. One key mitochondrial function is oxidative phosphorylation, which requires the coordinated function of several large mitochondrial complexes. The mitochondrial electron transport chain (mETC) is a series of complexes embedded in the inner mitochondrial membrane (IMM), named complex I (NADH dehydrogenase), complex II (succinate dehydrogenase), complex III (cytochrome bc_1 complex) and complex IV

(cytochrome *c* oxidase). These complexes are required to transfer electrons harvested from a variety of metabolic pathways to oxygen. This process is coupled with proton translocation across the inner mitochondrial membrane, creating an electrochemical gradient which is utilised by complex V (F_1F_o-ATP synthase) to generate ATP [2]. While most subunits of the mETC are encoded in the nucleus and imported into the organelle, several key subunits are encoded by the mitochondrial genome. They therefore require another mitochondrial complex, the mitochondrial ribosome (mitoribosome), for their translation. Mitochondrial complexes thus enable many core functions of the organelle.

Historically, most mitochondrial research was focused on oxidative phosphorylation and mitochondrial translation in a small group of model organisms that are closely related to one another, primarily mammals and yeast, resulting in an incomplete view of mitochondrial biology. However, recent research, particularly in unicellular eukaryotes, has started revealing that mitochondrial biology displays considerable diversity [3].

The Myzozoa are a group of unicellular eukaryotes which contains both parasitic and free-living species [4,5]. Parasitic lineages include species that have a huge impact on global health, the economy and the environment. For example, the phylum Apicomplexa brings together parasites that cause global diseases of both humans and livestock, most notably the malaria and toxoplasmosis caused by *Plasmodium* spp. and *Toxoplasma gondii*, respectively. Another example are the perkinsids, marine parasites that infect molluscs, including oysters, causing significant economic and environmental impact [6]. Myzozoans also include lineages that contain free-living algae and coral symbionts, such as the chrompodellids and dinoflagellates [4].

Recent studies showed that the apicomplexans display mETC and F_1F_o-ATP synthase complexes that are highly divergent from previously studied systems, both in composition and structure. All members have lost complex I, and there have been multiple parallel losses of mETC complexes in numerous lineages [7,8]. Of those that retain mETC complexes, including *Plasmodium* and *Toxoplasma*, the individual complexes have inflated subunit compositions compared to canonical complexes and display unique structures [9–16]. Importantly, a similar pattern is seen for F_1F_o-ATP synthase [10,11,17–19]. These new subunits correlate with novel features and functions of the corresponding complexes. For example, clade-specific subunits mediate ATP synthase hexamerization which is important for cristae formation [17], and mETC supercomplex formation [9]. Likewise, apicomplexan mitoribosomes are substantially distinct from their homologs in other eukaryotes. While apicomplexan mitochondrial genomes encode the lowest number of protein-coding genes known [20], their ribosomal RNAs (rRNAs) are uniquely extremely fragmented [21,22]. In *Toxoplasma* numerous clade-specific proteins take place in mitigating the extreme rRNA fragmentation, many of which seem conserved across the Myzozoa [23,24].

Through proteomic and structural investigations, we now have a much clearer understanding of apicomplexan mitochondrial complexes. However, we know close to nothing about the other myzozoan lineages. Intriguingly, many of the apicomplexan-specific subunits have putative homologs in these other lineages, hinting at clade-wide conservation. To gain a fuller picture of myzozoan mitochondrial biology, here we investigate mitochondrial complexes in a non-apicomplexan group. We chose to examine the marine parasite *Perkinsus marinus*, the best-studied member of the perkinsids, which is a sister clade to the dinoflagellates [4]. Perkinsids diverged close to the split with the clade containing apicomplexans and chrompodellids, making it a suitable sampling point for myzozoan diversity. Additionally, recent genetic and cell biology studies [25,26] make *P. marinus* a tractable model that will enable answering questions emerging from this work.

Here, we applied proteomic complexome profiling to *P. marinus* in order to gain a broad view of the protein composition of its mitochondrial complexes and understand the conservation of highly divergent organellar features across myzozoans.

Results

Isolation of *Perkinsus* mitochondria

Complexome profiling has proven a powerful proteomic technique for uncovering the composition of organellar protein complexes [27–29]. To study the mitochondrial complexes of *P. marinus*, we decided to take a dual approach, performing complexome profiling on both mitochondrially-enriched and whole-cell material.

To isolate material enriched in mitochondria, *P. marinus* cells (strain ATCC 50983) were lysed *via* mechanical disruption using glass beads, followed by differential centrifugation to enrich organellar material (see Materials and Methods). Immunoblot analysis of obtained fractions, using antibodies against the conserved ATP synthase beta subunit (ATPβ) (Fig 1A), confirmed mitochondrial enrichment. Antibodies against both a universally conserved cytosolic glyceraldehyde 3-phosphate dehydrogenase (GAPDH) and a nuclear histone H3 showed a strong signal in the total fraction, but absence or a decreased intensity in the mitochondrial fraction (Fig 1A), in support of the removal of these cell compartments during purification. On the other hand, an endoplasmic reticulum (ER) protein, the chaperone BiP, was also present in the mitochondrial fraction, indicating co-purification with other organelles. These data suggest that the purification protocol was able to obtain material enriched in mitochondrial proteins.

Next, to test whether we have isolated mitochondrial material suitable for complexome profiling, where intact complexes are required, we performed native-PAGE analysis. The mitochondrial material was solubilised in the non-ionic detergent n-dodecyl β-D-maltoside (βDDM) and complexes were separated by size *via* blue-native polyacrylamide gel electrophoresis (BN-PAGE). Coomassie staining of the gel showed numerous, clear, high-molecular-weight bands representing large macromolecular complexes (Fig 1B). To screen for known mitochondrial complexes, we first performed in-gel histochemical stains to test for the activity of mETC complex II and complex IV. By applying the complexes II- and IV-specific stains, we observed activity bands at ~900 kDa and ~450 kDa, respectively (Fig 1B), suggesting that in *P. marinus* these complexes are significantly larger than those seen in mammalian or yeast systems and similar in size to those described from the best-studied apicomplexans, *Plasmodium* and *Toxoplasma* [10,11]. We next performed immunoblot analysis with the ATPβ antibody to detect the F_1F_o-ATP synthase complex. We observed a high molecular weight band above 1 MDa (Fig 1B), suggesting a large complex of similar size to that seen in the apicomplexan parasites [10,17,30]. Additional low-molecular-weight bands were observed, perhaps reflecting monomeric ATPβ or assembly intermediates. Thus, BN-PAGE analysis indicates that the mitochondrially-enriched samples are suitable for further complexome analysis and suggests that *Perkinsus* possesses oxidative phosphorylation complexes that are divergent from commonly studied models and potentially similar to other myzozoans.

To investigate the composition of protein complexes within the whole-cell, *P. marinus* cells (strain PRA-240 (CB5D4;[31]) were lysed in a buffer containing the detergent IGEPAL *via* mechanical disruption with glass beads and the whole-cell protein content was separated in a BN-PAGE gel for complexome analysis.

130

131 Complexome profiling of *Perkinsus* mitochondrial complexes

132 We then proceeded to perform complexome analysis on both the mitochondrially-enriched material
133 and the whole-cell lysate. The mitochondrially-enriched fraction was treated with 1.7% βDDM to
134 solubilise membrane complexes, which were then separated by BN-PAGE, stained with Coomassie,
135 and the gel lane was cut into 60 gel slices (S1A Fig). Each gel slice was then analysed by mass
136 spectrometry and proteins identified using the Uniprot UP000007800 proteome annotation,
137 supplemented with the sequences of mitochondrially-encoded proteins [25]. Abundance data for
138 every protein for each of the remaining 60 gel slices was calculated using the iBAQ method, before
139 normalisation and hierarchical clustering was performed to generate the complexome profile [32,33].
140 Two independent complexome profiles, performed with separate mitochondrial isolations, were
141 generated (S1 Table). Between the two replicates, 4,243 individual proteins were detected, with 2,835
142 common to both datasets (S1B Fig; S1 Table). Further analysis was performed only on proteins
143 detected in both datasets, unless stated otherwise. Two sets of molecular weight markers were run in
144 parallel with the *Perkinsus* material: one composed of soluble proteins and the other containing
145 bovine mitochondrial membrane complexes (S1A Fig). This allowed mass calibration based on the
146 migration of both soluble and membrane-embedded proteins (S1A,C Fig; S3 Table).

147 For the whole-cell sample, proteins were solubilised in 0.1% IGEPAL, a milder non-ionic detergent, in
148 order to detect weaker inter-complex interactions. Protein complexes were separated by BN-PAGE
149 and the gel was excised into 48 slices (S1A Fig). Samples were analysed as above, with 3,552 proteins
150 detected (S1B Fig; S2 Table). Between the three datasets 1,747 proteins were detected in common
151 (S1B Fig; S1, S2 Tables), with 1,331 detected only in the whole-cell dataset, indicating differential cell
152 component enrichment between the two sample types, as would be expected. A ladder composed of
153 soluble proteins was run in parallel, allowing mass calibration (S1A,C Fig; S3 Table).

154 Next, to assess whether our complexome datasets had good coverage of the mitochondrial proteome
155 we compared it to organellar datasets from other myzozoan species. We first compared our two
156 mitochondrially-enriched complexome datasets to the hyperLOPIT spatial proteomics data from
157 *Toxoplasma* [34]. Our datasets contained putative *Perkinsus* homologs of between 64-67% of the
158 *Toxoplasma* proteins found in the mitochondrial clusters. This includes 67-70% of proteins belonging
159 to the "mitochondrial membranes" cluster. Our whole-cell sample contained putative homologs of
160 46% of proteins in the mitochondrial clusters. Finally, comparisons to a curated mitochondrial
161 proteome from *Plasmodium falciparum* [35] showed our mitochondrially-enriched complexome
162 datasets contained homologs of between 57-60% of *Plasmodium* mitochondrial proteins, while the
163 whole-cell dataset contained 38% of them. Overall, these comparisons suggest our complexome
164 profiles have sufficient coverage of mitochondrial proteins, suitable for assessing mitochondrial
165 complex composition.

166

167 Mitochondrial electron transport chain complexes

168 The multi-subunit complexes of the mETC show considerable compositional diversity across
169 eukaryotes, and recent studies in apicomplexans suggest a much-expanded subunit repertoire
170 compared to the commonly studied opisthokont models [2,3]. In order to determine whether this
171 expanded subunit repertoire extends to other myzozoans, we interrogated our *Perkinsus* complexome
172 datasets for mETC complexes.

173 We first searched for complex II subunits. While canonically a 4-subunit complex in the bacterial
174 ancestor and in well-studied models such as yeast and mammals, other lineages contain substantially
175 enlarged complexes. For example, plants possess an 8-subunit complex [36], the kinetoplastid
176 *Trypanosoma cruzi* has a 12-subunit complex [37], and in the ciliate *Tetrahymena* this complex consists
177 of 15 subunits [38]. Recent studies in apicomplexans found an 8-9 subunit complex in *Plasmodium* and
178 *Toxoplasma,* respectively [10–13], and its enlargement in *Eimeria* was also suggested [16]. All complex
179 II compositions possess two conserved matrix-facing subunits, SDHA and SDHB, that form the soluble
180 enzymatic domain that contains the FAD and Fe-S cofactors, as well as between 2 and 13 membrane-
181 embedded subunits that anchor the complex to the IMM. In the "canonical" enzyme those subunits
182 are named SDHC and SDHD and they further house the ubiquinone binding site. The amino acids
183 involved in ubiquinone binding in eukaryotes with enlarged subunit number have not yet been
184 experimentally characterized.

185 Searching our mitochondrially-enriched complexome dataset for the profiles of homologs of the highly
186 conserved SDHA and SDHB subunits identified proteins with a peak at both high molecular weight
187 (~900-990 kDa) and low molecular weight (between ~60 and 120 kDa) (Fig 2A, S4, S5 Tables). The low-
188 molecular-weight peak likely reflects either an assembly intermediate of the soluble matrix domain or
189 subunit monomer migration, while the one occurring at high molecular weight represents the mature
190 complex. This size of complex II is consistent with the BN-PAGE in-gel stain (Fig 1B). The whole-cell
191 complexome dataset also revealed evidence of a sub-assembly containing SDHA and SDHB migrating
192 at ~320-350 kDa (Fig 2B). Within the enriched mitochondrial dataset, 6 proteins that are homologs of
193 the recently identified apicomplexan membrane-anchoring complex II subunits (Fig 2A) peak at ~900
194 kDa. In the whole-cell complexome, these subunits migrated at high molecular weight of ~1290 kDa
195 (Fig 2B). These findings provide support for an affiliation of these 6 proteins as subunits of complex II
196 in *Perkinsus*. Their assignment to complex II is further supported by a recent structural study of the
197 mETC supercomplex in *Perkinsus* that identified them as part of a 10-subunit complex II [39].

198 We next searched for complex III subunits. In the mitochondrially-enriched complexome dataset, the
199 mitochondrially-encoded cytochrome *b* subunit was found with a peak at ~900 kDa (Fig 2A). Among
200 other proteins with a peak in the same slice, we found 8 other putative complex III subunits, identified
201 based on the homology to known apicomplexan subunits and to those identified in the recent mETC
202 supercomplex structure [39]. Searching the whole-cell complexome dataset identified 8 of these
203 subunits as migrating in the same gel slice providing additional support to their affiliation (Fig 2B).
204 Notably, in both datasets we found subunits of both complexes II and III predominantly migrating in
205 the same gel slice.

206 Additionally, we observed Pmar_PMAR021073, a predicted homolog of the complex III assembly factor
207 BCS1, with a peak in the gel slice below mature complex III, at ~820 kDa, and with high levels also
208 within the complex III gel slice (S1 Table). In other systems, BCS1 is involved in the maturation of the
209 Rieske (RIP1) subunit of complex III and is found in a late stage of assembly [40], suggesting that in our
210 mitochondrially-enriched complexome, we observe a late assembly intermediate as well as mature
211 complex III. Evidence of a lower molecular weight sub-assembly of complex III subunits QCR1 and
212 QCR2 are seen in both datasets as well (Fig 2A,B).

213 Complex IV has shown considerable variation in subunit number across the eukaryotes. Apicomplexans
214 possess an enlarged complex with 25 subunits, compared to just 14 observed in mammals [9]. The
215 recent *Perkinsus* mETC supercomplex structure suggests a 27-subunit complex [39]. We first searched
216 for the mitochondrially-encoded CoxI and CoxIII subunits and found them with a peak in a gel slice
217 representing ~420 kDa (Fig 2A; S4 S5 Tables). Moreover, this size of complex IV is consistent with the
218 BN-PAGE in-gel stain (Fig 1B). We detected 24 of the expected subunits in the same gel slice, thereby

219 confirming complex IV's composition (Fig 2A). Interestingly, we were not able to detect Cox2c, which
220 was observed in the *Perkinsus* structure, and its homolog was found in a recent structural study from
221 *Toxoplasma* [9]. However, this subunit has not been detected in numerous proteomic studies of the
222 apicomplexan mETC [3,15,28], suggesting challenges in its detection by mass spectrometry. Searching
223 the whole-cell complexome dataset identified CoxI and 21 further complex IV subunits, migrating at
224 high molecular weights and with up to three peaks of abundance, likely relating to multimers or
225 supercomplex formation (see below) (Fig 2B).

226 Associations between individual mETC complexes, termed supercomplexes, have been observed in
227 numerous systems, recently including Apicomplexa [9]. Likewise, the above-mentioned *Perkinsus*
228 structural study described a supercomplex composed of complexes II, III and IV (II2-III2-IV2) [39]. We
229 interrogated our datasets to see if we could detect any supercomplex. In the complexome from
230 mitochondrially-enriched samples, complexes II and III are found co-migrating, but subunits of
231 complex IV are not present in this gel slice. This is not unexpected, as the βDDM extraction does not
232 typically retain weaker inter-complex associations. The association of complexes II and III could be due
233 to the tight binding conferred by a long helical extension in SDHG observed in the structure [39]. We
234 therefore interrogated our whole-cell dataset, extracted in 0.1 % IGEPAL, which is more likely to retain
235 weaker inter-complex interactions. Here we observed that subunits from complexes II, III and IV
236 indeed appear together in multiple peaks of high relative abundance (Fig 2B, C). For example, complex
237 IV subunits have peaks at ~760-840, ~1,300-1,400 and ~2,800 kDa. Moreover, the peaks from different
238 respiratory complexes overlap, consistent with the detection of a supercomplex containing complexes
239 III and IV (Fig 2C).

240 Our complexome datasets allow identification of almost complete mETC complexes, validating their
241 composition, and demonstrating that the enlarged mETC complexes observed in Apicomplexa are
242 conserved across a broader group within the myzozoans and thus likely evolved in their common
243 ancestor.

244

245 <u>Evidence of interaction between complex III and putative inhibitors</u>

246 A structural study of the *Perkinsus* mETC supercomplex [39] identified two novel proteins that interact
247 with the RIP1 subunit of complex III. These proteins were proposed to act as inhibitors of the complex's
248 enzymatic activity due to their interaction site overlapping with the binding site for cytochrome *c*.
249 These proteins were named ISPR1 and ISPR2 (for Iron-Sulfur Protein Related). To lend support to this
250 observation we searched for them in our complexome datasets. Both proteins were detected in both
251 replicates of our complexome on mitochondrially-enriched samples. Major peaks were identified at
252 low molecular weight slices likely representing free monomers or dimers. However, in the second
253 replicate a secondary, smaller, peak was detected in gel slices that contains complex III subunits (Fig
254 2D), consistent with an interaction between ISPR1, ISPR2 and this complex.

255 The identification of a novel complex III inhibitory factor in *Perkinsus* raises the question of whether it
256 is a lineage-specific innovation, or if it is more widely conserved. It was noted that *Toxoplasma* contains
257 a likely homolog, TGGT1_224932 [39]. To test if the mitochondrial localisation of this putative *Tg*ISPR
258 is conserved, we exogenously expressed a Ty epitope-tagged version of the protein in *Toxoplasma*
259 under the tubulin promoter and performed immunofluorescence analysis. We observed signal with a
260 characteristic mitochondrial "lasso-shape" morphology [41], which co-localised with the
261 mitochondrial marker TOM40 [42], supporting mitochondrial localisation (Fig 2E). Future functional
262 studies will be required to determine whether *Tg*ISPR performs an inhibitory role as proposed for

263 *Perkinsus*. Overall, our results lend support to the observation that novel proteins interact with
264 complex III in *Perkinsus* and lays the foundation for future functional investigations in the
265 apicomplexan models.

266

267 Detection of F_1F_o-ATP synthase

268 In *Toxoplasma* F_1F_o-ATP synthase complex is a huge 1.85 MDa complex consisting of 32 subunits
269 [10,17–19], compared to ~15 canonical subunits of the yeast and mammalian systems. Immunoblot
270 analysis (Fig 1B) provides hints that *Perkinsus* possesses a similarly enlarged ATP synthase. Searching
271 for homologs of confirmed *Toxoplasma* ATP synthase subunits within the *Perkinsus* genome identified
272 27 putative homologs (S4 Table). Of these, 26 were present in our mitochondrially-enriched
273 complexome dataset and 25 in the whole-cell dataset. The conserved subunit c is an expected
274 exception, as it has previously proved recalcitrant to detection by mass spectrometry [18]. All 26
275 subunits peaked in relative abundance at ~1.9 MDa in the mitochondrial complexome (Fig 3A; S4, S5
276 Tables), and at ~1.5 MDa in the whole-cell complexome (Fig 3B), confirming an enlarged ATP synthase.
277 Conserved subunits include ATPTG8 and 9, which contain coiled-coil-helix-coiled-coil-helix (CHCH)
278 domains. Subunits containing CHCH-domains have recently been shown to be essential for ATP
279 synthase formation [43] and were previously only studied in apicomplexans. Their presence in
280 *Perkinsus* suggests CHCH-domain containing ATP synthase subunits are a myzozoan-wide feature. The
281 ATP synthase inhibitor subunit IF1 was found also in a secondary low-molecular-weight peak,
282 consistent in size with monomer or dimer migration, and providing evidence that the IF1 pool is not
283 permanently engaged with the mature complex. Likewise, the conserved catalytic subunit ATPβ also
284 has a low molecular weight peak, matching the secondary band seen by immunoblot analysis (Fig 1B).

285 We were unable to identify *Perkinsus* homologs of many of the lineage-specific lumen-facing subunits
286 identified from the *Toxoplasma* structure (ATPTG5,7,10,11,16) (Fig 3C). *Perkinsus* may lack an
287 expanded luminal domain, or possesses derived versions of the missing subunits, which we were not
288 able to detect by homology searches due to sequence divergence. To explore further we searched our
289 complexome for co-migrating proteins which may be novel subunits. We noted that, in all complexome
290 datasets, 2 other proteins (Pmar_PMAR021141 and Pmar_PMAR014495) consistently co-migrated
291 with the other subunits of ATP synthase, with similar abundance to other myzozoan-specific ATP
292 synthase subunits (Fig 3A, B, D). Similar to the missing subunits from *Toxoplasma* ATPTG10,11 and 16,
293 Pmar_PMAR021141 is a short protein of 10 kDa. Pmar_PMAR014495 is a 19 kDa protein with a
294 predicted thioredoxin domain (Fig 3E). To investigate further, we first purified ATP synthase by size
295 exclusion chromatography and submitted it for mass spectrometry analysis (S2A, B Fig). In addition to
296 detection of 22 expected ATP synthase subunits, both of these new proteins were also present (S6
297 Table). These data suggest that they are genuine ATP synthase subunits, and we putatively assign them
298 the names ATPPM1-2, although further experimental work would be required to confirm this.
299 Combined, these data confirm that *Perkinsus* has an enlarged ATP synthase, and that this divergent
300 complex is conserved across sampled myzozoans and reveals putative new species-specific subunits.

301 It was previously observed in *Toxoplasma* that the gene encoding ATP synthase subunit ATPTG1 also
302 separately encodes the complex III subunit CytC1, suggesting post-translational cleavage [10] and
303 potentially coupled assembly of the mETC and ATP synthase [44]. Homology analysis showed that this
304 fusion was conserved across a subset of apicomplexans and that outside this group ATPTG1 and CytC1
305 are encoded by separate genes [10] (S3C, D, S4 Figs). Our detection of ATPTG1 in complex with ATP
306 synthase strongly suggests a role for this protein as an ATP synthase subunit prior to the fusion event
307 with CytC1.

308

309 Mitochondrial ribosome

310 The mitoribosome is a macromolecular complex required to translate transcripts encoded by the
311 mitochondrial genome, consisting of two large riboprotein subunits – the large (LSU) and small subunit
312 (SSU). Both the LSU and SSU are composed of numerous proteins and rRNAs. In the myzozoan lineage,
313 the mitochondrial genomes predict an unusually fragmented rRNA backbone [5,20,21,45], which
314 would require the function of new proteins to support translation. Two recent structural studies of
315 *Toxoplasma* confirmed this hypothesis and demonstrated that, similarly to mETC and ATP synthase,
316 apicomplexans have mitoribosomes that diverge significantly from their better studied homologs in
317 humans and yeast [23,24]. Notably, the *Toxoplasma* mitoribosome contains at least 124 subunits (73
318 in LSU, 51 in SSU), including 55 clade-specific ones [23]. In contrast, the yeast and human
319 mitoribosomes contain in total only 75 and 80 subunits, respectively [46,47]. This difference supports
320 the notion that the recruitment of this group of unorthodox mitoribosomal proteins acts to mitigate
321 the highly fragmented rRNA.

322 To test if this divergent composition is conserved across myzozoans, we first searched for homologs of
323 confirmed *Toxoplasma* mitoribosomal proteins within the *Perkinsus* genome, and identified 78
324 putative homologs (S4 table). Of these, 74 were identified in at least one complexome dataset. In the
325 first replicate of the mitochondrial complexome, 70 subunits were detected, with 67 of them showing
326 their highest abundance in the top gel slices (~ 2 MDa) (Fig 4). The LSU and SSU subunits were observed
327 most prominently in the top two and three gel slices, respectively. This slight difference in migration
328 could represent separate migration of the LSU and SSU, or a mixture between full monosomes and
329 individual subunits. We observed 21 of the 55 clade-specific subunits co-migrating with the
330 mitoribosome, suggesting partial conservation across myzozoans. In the whole-cell complexome, we
331 detected 18 out of 74 putative subunits, 5 from the SSU and 13 from the LSU (S5 Table). The lower
332 number of detected proteins potentially reflects different detergent extraction conditions used in the
333 mitochondrial dataset, leading to the differential preservation of higher-order molecular interactions.
334 As observed in the mitochondrial dataset, the LSU and SSU proteins possess slightly different migration
335 profiles, with 7 out of 14 LSU proteins showing their highest peak at ~1.7 MDa, while 4 out of 5
336 detected SSU factors migrate mainly above 2 MDa.

337 Structural analyses of the *Toxoplasma* mitoribosome revealed the extent of rRNA fragmentation and
338 provided insight into the mechanism through which lineage-specific proteins mitigate this
339 fragmentation and promote ribosomal function through RNA-protein interactions [23]. For example,
340 11 *Toxoplasma* proteins interact each with multiple rRNAs and therefore were assigned a putative role
341 as "joints". *Perkinsus* is also thought to contain highly fragmented rRNAs [25]. We detected 8 of the 11
342 joint proteins, suggesting conservation in the architecture of protein scaffolds for supporting rRNA
343 fragment stability and formation of critical mitoribosomal functional domains. This included a RAP
344 (**R**NA-binding domain abundant in **ap**icomplexans) domain-containing protein homologous to
345 *Toxoplasma* mL138, which is essential for mitoribosome stability [23]. Five RAP domain proteins were
346 found in the *Toxoplasma* mitoribosome with this suggested regulatory role, three of which (mL136,
347 mL138 and mL147) are conserved in *Perkinsus* and migrate with the mitoribosome.

348 Myzozoan genomes encode proteins with the AP2 transcription factor domains. In the apicomplexans,
349 numerous members of this family (called ApiAP2) are involved in controlling gene expression-
350 dependent life cycle stage transitions [48]. Surprisingly, in *Toxoplasma,* 4 out of 67 ApiAP2 proteins,
351 have been incorporated into the mitoribosome [23,24]. *Perkinsus* has 25 predicted ApiAP2
352 proteins[49], 4 of which migrate with the mitoribosome (mS130, mL143, mL153, mL161) (Fig 4; S5

353 Table). This suggests that the unusual incorporation of AP2-like proteins in the mitoribosome is
354 conserved across the myzozoans. Additionally, the *Toxoplasma* mitoribosome contains proteins with
355 domains that may indicate repurposing from another function. Two examples include mL151, which
356 has a BolA-like domain, commonly found in the iron-sulfur cluster assembly pathway proteins, and
357 mS134, which has an acylphosphatase enzymatic domain. Both proteins appear conserved as
358 mitoribosomal components in *Perkinsus* as their homologs peak together with the other
359 mitoribosomal proteins.

360 Overall, several unusual features recently observed in *Toxoplasma* mitoribosome appear conserved in
361 *Perkinsus*, suggesting that these innovations are Myzozoa-conserved. Future structural studies will be
362 needed to unravel the full extent of conservation of these features, and any unique attributes of the
363 *Perkinsus* mitoribosome.

364

365 Complexes from other cell compartments

366 Finally, we explored whether our complexome datasets could provide insight into other cell
367 compartments. We reasoned that our whole-cell complexome would provide cell-wide coverage, and,
368 as previously highlighted, immunoblot analysis of fractions from our mitochondrial purification
369 protocol suggested co-purification of other organelles (Fig 1A). We first investigated the 26S
370 proteasome complex. Homology searches identified *Perkinsus* homologs of 32 out of 33 subunits from
371 the human complex [50]. We could identify 17 subunits of the 19S proteasome/ regulatory particle
372 migrating at 1.4 MDa in our mitochondrial complexome, and 16 subunits migrating at 1.2 MDa in our
373 whole-cell complexome (Fig 5A, B). Similarly, we could detect 14 subunits of the 20S proteasome/core
374 particle migrating at 690 kDa in our mitochondrial complexome and 13 subunits migrating at 765 kDa
375 in our whole-cell complexome. Detection of the proteasome was also observed in a previous
376 mitochondrial complexome of *Plasmodium falciparum* [11].

377 Since immunoblot analysis suggested co-purification of the endoplasmic reticulum, we searched our
378 mitochondrial complexome for the endoplasmic reticulum membrane protein complex (EMC). We
379 identified in *Perkinsus* clear homologs of 7 of the 9 human subunits [51], which migrated at 330 kDa
380 in our mitochondrial complexome (Fig 5C). Recently, this complex was also identified in the
381 *Plasmodium* complexome [11]. Interestingly, unlike in *Plasmodium*, we were able to detect the EMC6
382 subunit migrating with other EMC components.

383 Detection of the proteasome and EMC suggests our datasets are suitable for exploring the composition
384 of macro-molecular protein complex in other cellular compartments, and may provide extra insight
385 and comparison to future spatial proteomic studies.

386

387 Discussion

388 Mitochondria are unique and defining features of the eukaryotic cell and play a variety of important
389 roles in their function. However, our knowledge of how they operate is largely derived from a narrow
390 set of model organisms that are often closely related. Indeed, the vast majority of eukaryotic diversity,
391 especially in mitochondrial biology, is “hidden” in unicellular eukaryotes and, despite increased recent
392 research efforts, we still know surprisingly little about their molecular features.

393 An example of the diversity of mitochondrial functions across the eukaryotes is in the variety of
394 mitochondrial proteomes. The size of an organism’s mitochondrial proteomes is often indicative of

395 the organism's mitochondrial capacity [52]. Unicellular eukaryotes offer examples from both ends of
396 this spectrum. For example, the most complex mitochondrial proteomes to date come from the
397 euglenid *Euglena gracilis* and *Paradiplonema* (alternatively referred to as *Diplonema*) *papillatum* with
398 estimated ~1,800 and ~1,900 proteins [53]. At the other end of the spectrum, the mitochondria of
399 other protists have been subject to massive reduction [54], including some that have dispensed with
400 mitochondria altogether [55]. Indeed, parasitic lineages are well known for streamlining their
401 genomes [56], which likely provides spatial efficiency and energy conservation [57], with the
402 mitochondria being a clear example of this trend. The greatest diversity of mitochondrial biology is
403 therefore found in unicellular eukaryotes [58].

404 One area in which this diversity manifests itself is in the composition and features of the mitochondrial
405 complexes involved in oxidative phosphorylation. Over the past few years, a number of studies in a
406 variety of protist lineages have shown considerable divergence in the composition and features of
407 these mitochondrial complexes in comparison to the "textbook" model systems, such as yeast and
408 mammals. A stark example comes from recent structural studies of the ciliate *Tetrahymena*
409 *thermophila* that demonstrated a respiratory chain composed of ~150 proteins compared to ~90 in
410 humans [38,59–61]. Similar findings have been found in the apicomplexans. The mitochondrial
411 complexes of this lineage have been the subject of sustained research effort in the past decade, largely
412 due to their global importance as pathogens of humans and livestock, and their development as
413 powerful tractable model organisms. Through both proteomic and structural approaches, it has been
414 shown that almost every mitochondrial complex is substantially larger than the opisthokont version,
415 contrary to the simplified yet prevailing notion that parasite pathways are reduced compared to their
416 host. These observations span complex II [10–13], complex IV [9–11,15]and ATP synthase [10,11,17–
417 19]. The larger size is an outcome of numerous species or clade-specific subunits, and the field is still
418 exploring the driving forces for their recruitment.

419 Despite this progress, it was still unclear if the newly discovered subunits were specific to the
420 apicomplexans, or more widely conserved across other related lineages within the myzozoa. Here, we
421 aimed to answer this question by exploring the mitochondrial complexes of an early-diverging
422 myzozoan, *P. marinus*. Our focus on the Perkinsozoa clade, which is sister group to the dinoflagellates,
423 and branched from the lineage that forms apicomplexans and chromerids early in myzozoan
424 evolution, allows insight into the evolution of these features from the ancestral state. Shared
425 mitochondrial features found here would suggest their emergence prior to the split and, importantly,
426 prior to the shift to parasitism in Apicomplexa.

427 Our findings broadly point to a conservation of mitochondrial complex composition both for the
428 oxidative phosphorylation complexes and the mitoribosome. Novel innovations first observed in the
429 apicomplexan parasites, for example the enlarged subunit composition of complexes II and IV, and
430 ATP synthase, as well as the addition of novel proteins to the mitoribosome, are observed in *Perkinsus*,
431 consistent with conservation across myzozoans. This suggests a scenario where the last common
432 ancestor of the 4 diverging lineages, namely dinoflagellates, chromerids, apicomplexans and
433 perkinsozoans, already possessed enlarged mitochondrial complexes consisting of many of the clade-
434 conserved and -specific subunits seen in both parasites. Given the number of free-living species in
435 these lineages, and the multiple independent origins of parasitism, this would also imply this feature
436 is unrelated to a parasitic lifestyle.

437 A question that naturally arises is how these enlarged complexes in unicellular eukaryotes arose and
438 what purpose the additional subunits play. We do not have definitive answers, but several reasons
439 can be discussed. In some cases, numerous subunits with reduced hydrophobicity provide the
440 structural features of a single more hydrophobic subunit, and it has been hypothesised that reduced

441 mitochondrial genome content is a driving force for this outcome [9,17,39,62], as they allow transfer
442 of subunit-encoding genes from the mitochondrial to nuclear genome [63]. This process may be aided
443 by splitting up of large hydrophobic proteins, that would prove problematic for mitochondrial import,
444 into more numerous, less hydrophobic, subunits [10]. Another theory is that these extra subunits
445 imbue the complex with additional functions. Structural studies revealed that, in many cases, species-
446 or clade-specific subunits mediate interactions between complexes and multimerization of
447 complexes, which seem to evolve in line with the shape of mitochondrial cristae [9,17,38]. An example
448 of this is the additional subunits in *Toxoplasma* ATP synthase, which allow the formation of hexamers,
449 with a role in shaping the cristae membrane [17]. Likewise, in the formation of *Toxoplasma*
450 supercomplex, complexes III and IV interact in an alternate orientation from mammals, and this novel
451 interaction interface is lined with the lineage-specific subunits [9]. In *Perkinsus*, the novel subunit,
452 SDHG, appears to promote close associations between complexes II and III, perhaps aiding in
453 supercomplex stability [39]. Extra subunits have also been proposed to play a role in maintaining
454 complex stability in mitoribosomes [23,64,65]. The reason for a largely increased repertoire of
455 accessory subunits may be a combination of (all) the above.

456 Our study revealed a number of components conserved between the *Perkinsus* and the *Toxoplasma*
457 mitoribosomes, indicating that they potentially share many of the unusual features recently
458 uncovered in the apicomplexans [23,24]. The unique mitoribosomal rRNA fragmentation is common
459 to all myzozoans whose mitochondrial genomes have been sequenced [22,25,66] and, therefore, it is
460 likely that features that evolved to "mend" the fragments, control assembly, and maintain stability are
461 also shared. Structural observations derived from the *Toxoplasma* mitoribosome, the only one
462 available for myzozoans, pointed out three main features that have the potential to mitigate the
463 extreme rRNA fragmentations: i) proteins that binds several rRNA molecules and thus act as "joints";
464 ii) high abundance of short peptides that are enriched with aromatic residues capable of stacking with
465 nucleobases and with charged residues able to interact with backbone rRNA, thus promoting
466 association between rRNA molecules; and, iii) the addition of poly-A tails onto rRNA that are bound
467 by proteins, which in return bind each other, promoting indirect association between rRNAs. The
468 *Perkinsus* mitoribosome peak contains homologs of "joint" proteins, but we were unable to identify
469 homologs of the short peptides which promote association of short rRNAs. This may imply a different
470 mitigation solution for dealing with short rRNAs has evolved in *Perkinsus*. Alternatively, short peptides
471 may be present that have extensively diverged from *Toxoplasma* making them hard to detect by
472 homology searches. Likewise, homologs of the proteins that bind to poly-A tails migrate with other
473 *Perkinsus* mitoribosomal proteins suggesting that this mechanism is also conserved. This is further
474 supported by the identification of a homolog of TgmtPAP1, which is a mitochondrial poly-A
475 polymerase important for the complete polyadenylation of mitoribosomal rRNA in *Toxoplasma* [23].

476 The observation that 4 members of the ApiAP2 transcription factor family are integral mitoribosome
477 components in *Toxoplasma* [23,24] is extended here to *Perkinsus*. However, while *Toxoplasma* has an
478 unusually expanded number of apiAP2 family members, 67 in total, the *Perkinsus* genome encodes
479 only 25 [49], and 4 of them are mitoribosomal. Homologs of those 4 ApiAP2 are found across the
480 myzozoan clade including dinoflagellates, in which 5 have been detected. It is tempting to hypothesise
481 that rRNA fragmentation and the acquisition of these 4 mitoribosomal proteins with ApiAP2 folds have
482 co-evolved; however, this requires further investigation.

483 Recent studies on the *Perkinsus* mitochondrial genome highlighted its several specific features,
484 including replacement of the canonical UGA stop codon to code for tryptophan, and an unusual
485 programmed ribosomal frameshifting found in all genes, which seems to require 18 to 19 corrections
486 across the encoded mitochondrial proteins [25]. These irregularities would necessitate adjustment in

487 mitoribosome functional control, and potentially result in the evolution and recruitment of *Perkinsus*-
488 specific proteins and features. We found numerous proteins, annotated as uncharacterised, co-
489 migrating with confirmed mitoribosomal proteins. Although we cannot currently provide support for
490 their mitoribosome affiliation, as some may belong to other high molecular complexes, it is likely that
491 many are *bona fide Perkinsus*-specific mitoribosome proteins. Structural studies would assist in
492 assigning any new proteins and revealing any *Perkinsus*-specific mitoribosome features.

493 *Perkinsus marinus* has proved a versatile model organism for understanding myzozoan biology and is
494 increasingly being utilised for investigations into divergent eukaryotic biology, of which this study is
495 an example. We applied a proteomic complexome profiling approach [27], which has proved a
496 powerful method for uncovering the composition of organellar complexes [28,29]. It has most
497 frequently been used for studying organelles in more commonly studied organisms, and significantly
498 contributed to our understanding of pathologies in mitochondrial disease patients [67], mammalian
499 [68] and yeast mitochondrial biology [69], and plant and algal organellar biology [70,71]. More
500 recently, it has also been successfully used for exploring non-model lineages. Recent complexome
501 studies of unicellular eukaryotes include *Plasmodium* [11], *Toxoplasma* [10], the extremophile yeast
502 *Rhodotorula mucilaginosa* [72] and this study. We believe complexome profiling will be a powerful
503 tool for future explorations of divergent mitochondrial biology.

504

505 ## Materials and methods

506 **Cell culture**

507 *Perkinsus marinus* cells (strain ATCC 50983), used the mitochondrially-enriched complexome, were
508 grown in liquid culture in ATCC medium 1886 supplemented with penicillin and streptomycin.
509 *Perkinsus marinus* strain PRA-240 (CB5D4; [31]), used for the whole-cell complexome, was grown in
510 modified DME:Ham's F12 (1:2) medium supplemented with 5 % foetal bovine serum, 50 mM HEPES,
511 3.6 mM sodium bicarbonate, 15 g/L artificial sea salts, 100 U/mL penicillin G, and 100 U/mL
512 streptomycin sulphate, pH 6.6. Cells were grown without agitation in the dark at 25-26 °C. For culture
513 maintenance, 200 µL of stationary-phase culture were transferred to a T25 culture flask with 10 mL of
514 fresh medium once a week.

515

516 **Isolation of mitochondrial material**

517 Enriched mitochondrial fractions were obtained by cell lysis followed by differential centrifugation.
518 *Perkinsus* cells were grown in ~1.5 L of liquid culture and harvested at OD_{600} ~1. Cells were pelleted by
519 centrifugation at 1000 x g for 15 minutes at 4 °C and weighed. Per gram of cells, 2 g fine glass beads
520 and 2 mL ice-cold mito-membrane buffer (0.6 M sucrose, 20 mM MOPS-NaOH, pH 7.5, 1 mM EDTA)
521 containing protease inhibitors were added. Cells were disrupted by 8 rounds of 1-minute vortexing
522 and 1-minute incubation on ice. Differential centrifugation was performed at 3,500 × *g* for 10 minutes
523 at 4 °C followed by 40,000 × *g* for 120 minutes at 4 °C. Pellets containing mitochondrial membranes
524 were stored at -80 °C before use.

525 **Preparation of whole-cell samples**

526 5 x 10^7 of cells (OD_{600} ~2) were harvested by centrifugation at 1,700 × *g* for 10 min at 4°C. The cell
527 pellet was resuspended in 50 µl of solubilization buffer (50 mM NaCl, 50 mM Bis-Tris/HCl pH 7.0, 2
528 mM 6-Aminocaproic acid (ACA), 1 mM EDTA) containing 0.1% IGEPAL CA-630 detergent and
529 supplemented with 1x complete EDTA-free protease inhibitor and 12.5 µg of 0.1% (w/v) DNase. 1 g of

530 fine glass beads were added, and cells were disrupted by vortexing for 3 min at 4°C. To remove unlysed
531 cells and insoluble material, the cell lysate was cleared by centrifugation at 1,000 × *g* for 10 min at 4°C.
532 Protein concentration was determined by the BCA protein quantification assay.

533 **Blue native, SDS PAGE and immunoblot analysis**

534 SDS-PAGE: 7.5 µg of protein lysate, measured using a Bradford assay, was resuspended in Laemmli
535 buffer (2% (w/v) SDS, 125 mM Tris-HCl, pH 6.8, 10% (w/v) glycerol, 0.04% (v/v) β-mercaptoethanol,
536 0.002% (w/v) bromophenol blue) and heated at 95 °C for 5 min. Proteins were then separated on a
537 12.5 % SDS-polyacrylamide gel. EZ-Run Prestained Rec protein ladder was used as a molecular weight
538 marker. Proteins were transferred under semi-dry conditions to a nitrocellulose membrane and
539 labelled with primary antibodies: anti-ATPβ (Agrisera AS05085, 1:5000), anti-histone H3 (Abcam
540 ab1791, 1:1,000), anti-GAPDH (Abcam ab125247, 1:2,000), anti-BiP (a gift from James D. Bangs,
541 1:5,000). This was followed by labelling with secondary fluorescent antibodies IRDye 800CW, 680RD
542 (1:10,000, LIC-COR) and detection with an Odyssey CLx. As a loading control, duplicate gels run in
543 parallel were incubated for 1 hr in instant blue.

544 Blue Native (BN) PAGE for mitochondrially-enriched samples:
545 Samples were resuspended in solubilization buffer containing 1.75 % βDDM, 750 mM aminocaproic
546 acid, 50 mM Bis-Tris-HCl (pH 7.0), 0.5 mM EDTA. This was followed by incubation on ice for 30 min
547 followed by centrifugation at 16,000 × *g* at 4°C for 30 min to separate solubilized protein complexes
548 from insoluble material. This supernatant was combined with sample buffer containing Coomassie
549 G250, resulting in a final concentration of 0.4375% βDDM and 0.1% Coomassie G250 and a protein:
550 detergent ratio of ~1: 5.8. 15-30 µg of sample was separated on a 4-16% Bis-Tris gel under native
551 conditions. Bovine mitochondrial membranes, as well as NativeMark were used as a molecular weight
552 marker.

553 To visualize total proteins, gels were incubated in a 0.1% (w/v) Coomassie R-250, 45% methanol (v/v),
554 10% acetic acid (v/v) solution, followed by de-staining and incubation in milliQ water. For immunoblot
555 analysis protein was transferred to a PVDF membrane and probed with anti-ATPβ as above. In-gel
556 histochemical stains were performed as in [73]. Briefly, for detection of succinate dehydrogenase the
557 gel was incubated in 50 mM KH_2PO_4, pH 7.4, 0.1 mM ATP, 0.2 mM phenazine methosulfate, 10 mM
558 succinate and 0.2% (w/v) nitroblue tetrazolium until the stain was observed, and the reaction stopped
559 and gel further destained by incubation in 45% methanol (v/v), 10% acetic acid (v/v). For detection of
560 cytochrome *c* oxidase activity, the gel was incubated with 50 mM KH_2PO_4, pH 7.2, 1 mg ml−1
561 cytochrome *c*, 0.1% (w/v) 3,3′-diaminobenzidine tetrahydrochloride until the stain was observed, and
562 the reaction stopped and gel further destained by incubation in 45% methanol (v/v), 10% acetic acid
563 (v/v).

564 For complexome profiling of mitochondrial-enriched material, a gel lane was cut into 60 gel slices (S1A
565 Fig), excluding the very top and bottom sections of the gel. These sections were processed separately
566 as they may contain aggregated proteins that would confound complexome analysis. Each slice was
567 further diced into small cubes to aid trypsin digestion.

568 Blue Native (BN) Page for whole-cell samples:
569 Two identical gels were run. For each of the two, 16.5 µL of cleared lysate containing 80 µg of protein
570 was mixed with 1.5 µL loading dye (5 mM ACA, 5% (w/v) Coomassie brilliant blue (CBB) R-250) and 2
571 µL 50% (v/v) glycerol and separated by BN PAGE in NativePAGE 3%-12% Bis-Tris gels. The
572 electrophoresis was performed in 200 mL of Blue Cathode Buffer (15 mM Bis-Tris/HCl pH 7.0, 50 mM
573 Tricine, 0.002% (w/v) CBB R-250) and 150 mL Anode Buffer (50 mM Bis-Tris/HCl pH 7.0) under the

following running conditions: a first step was performed at 80V and 15 mA for 10 min, followed by a second one at 100V and 20 mA for 3 hrs and 30 min, and finally a third one of additional 30 min at 130 V and 25mA. NativeMark was run along with the sample to estimate molecular weight sizes.
Gels were both fixed in 25% (v/v) methanol and 10% (v/v) acetic acid on a shaker for 1 hr, at room temperature, and rinsed multiple times in MilliQ water.

For complexome profiling of whole-cell material, a gel lane was excised into 48 1.5 mm slices (S1A Fig), and these were transferred into a 96-well filter plate for further processing.

In-gel trypsin digest

Mitochondrial samples: In-gel tryptic digestion was carried out on each gel slice. Briefly, diced gel slices were washed in 100 mM ammonium bicarbonate, followed by a wash in 50% acetonitrile and 100 mM ammonium bicarbonate. Cysteine reduction and alkylation were achieved *via* incubation in a solution of 45 mM DTT and 100 mM ammonium bicarbonate at 60 °C, followed by incubation in the dark with 100 mM iodoacetamide. Slices were washed again in 50% acetonitrile and 100 mM ammonium bicarbonate, followed by incubation in 100% acetonitrile. Trypsin digest was then performed overnight at 37 °C. Liquid was then removed from the gel slices and into to a 96-well microplate. The remaining gel slices were washed by incubation in 5% formic acid before the addition of acetonitrile, and the liquid transferred and pooled in the corresponding well of the microplate. Samples were then dried in a vacuum centrifuge, ready for MS analysis.

Whole-cell samples: Prior to the LC-MS analysis, protein digestion was performed on each gel slice. Briefly, gels were cut into smaller pieces and bleached with mixture of 50 mM ammonium bicarbonate (ABC) with acetonitrile (1:1 v/v). Gel was afterwards dried by pure acetonitrile and reduced with 10 mM DTT (dithiothreitol) in 100 mM ABC for 30 min at 60 °C. 55 mM chloroacetoamide in 100 mM ABC was added to the gel, incubated for 10 min at the room temperature and the gel was then washed twice with acetonitrile. Dry gel was mixed with trypsin that was resuspended in acetic acid, ABC and acetonitrile and incubated overnight at 37 °C. After digestion samples were mixed with 0.1% TFA in 60% acetonitrile and peptides were desalted using in-house made stage tips packed with C18 disks (Empore) according to [74].

Mass spectrometry

Mitochondrial samples: Dried peptide residues were solubilized in 20 µL 5 % acetonitrile with 0.5 % formic acid using the auto-sampler of a nanoflow uHPLC system (Thermo Scientific RSLCnano). Online detection of peptide ions was by electrospray ionisation (ESI) mass spectrometry MS/MS with an Orbitrap Fusion MS (Thermo Scientific). Ionisation of LC eluent was performed by interfacing the LC coupling device to a NanoMate Triversa (Advion Bioscience) with an electrospray voltage of 1.7 kV. An injection volume of 5 µL of the reconstituted protein digest were desalted and concentrated for 10 min on trap column (0.3 × 5 mm) using a flow rate of 25 µl / min with 1 % acetonitrile with 0.1 % formic acid. Peptide separation was performed on a Pepmap C18 reversed-phase column (50 cm × 75 µm, particle size 3 µm, pore size 100 Å, Thermo Scientific) using a solvent gradient at a fixed solvent flow rate of 0.3 µl / min for the analytical column. The solvent composition was A) 0.1 % formic acid in water, B) 0.08 % formic acid in 80% acetonitrile 20% water. The solvent gradient was 4 % B for 1.5 min, 4 to 60 % for 50.5 min, 60 to 99 % for 3 min, held at 99 % for 7 min. A further 13 minutes at initial conditions for column re-equilibration was used before the next injection. The Orbitrap Fusion acquired full-scan MS in the range 310 to 2000 *m/z* for a high-resolution precursor scan at 120,000 RP (at 200 *m/z*), while simultaneously acquiring up to the top 15 precursors were isolated at 0.7 *m/z*

width and subjected to CID fragmentation (35 % NCE) in the linear ion trap using rapid scan mode. Singly charged ions are excluded from selection, while selected precursors are added to a dynamic exclusion list for 30 sec.

Whole-cell samples: For LC/MS analysis, a Nano Reversed phase column (Ion Opticks, Aurora Ultimate XT C18 UHPLC column, 25 cm × 75 µm ID, 1.7 µm particles, 120 Å pore size, Ion Optics, Australia) was used for LC/MS analysis. Mobile phase buffer A was composed of water and 0.1% formic acid. Mobile phase B was composed of acetonitrile and 0.1% formic acid. Samples were loaded onto the trap column (C18 PepMap100, 5 µm particle size, 300 µm x 5 mm, Thermo Scientific) for 4 min at 18 µl/min loading buffer was composed of water, 2% acetonitrile and 0.1% trifluoroacetic acid. Peptides were eluted with mobile phase B gradient from 4% to 35% B in 15 min. Eluting peptide cations were converted to gas-phase ions by electrospray ionization and analysed on a Thermo Orbitrap Fusion (Thermo Scientific) by data dependent approach. Survey scans of peptide precursors from 350 to 1,400 m/z were performed in orbitrap at 120K resolution (at 200 m/z) with a 100 % ion count target. Tandem MS was performed by isolation at 1.6 Da with the quadrupole, HCD fragmentation with normalized collision energy of 30 % and 10 ms activation time. Fragmentation spectra were acquired in ion trap with scan rate set to Rapid. The MS2 ion count target was set to 150 % and the max injection time was 100 ms. Only those precursors with charge state 2–6 were sampled for MS2. The dynamic exclusion duration was set to 30 s with a 10-ppm tolerance around the selected precursor and its isotopes. Monoisotopic precursor selection was turned on. Cycle time was set to 1.5 s.

Complexome profiling

Complexome profiling was performed as described in [32,33] . Briefly, RAW mass spectrometry data files for each individual gel slice were analysed using MaxQuant (v2.0.3.0 or v2.4.13.0) [75], accessed using the Galaxy server [76], using default settings. For protein identification, peptides were searched against a custom database containing the *P. marinus* proteome (Uniprot UP000007800) and protein sequences for mitochondrial encoded proteins CoxI, CoxIII and CytB [25]. Protein abundance values were calculated using the iBAQ method and profiles analysed using Nova software (v0.5.8) [77]. Profiles were normalised using the maximum normalisation function and hierarchical clustering performed with the Pearson Correlation distance function. Heatmaps were visualised using GraphPad Prism software (v10.6.1).

Phylogenetic analysis

The ATPTG1 protein sequence from *P. marinus* (Pmar_PMAR013021) was used as a query in BLASTp search against the dataset of 132 alveolate species from EukProt database v.3[78] (S7 Table) with an *e*-value threshold of 1*e*-5. Retrieved sequences were aligned using MAFFT v.7.505 with the L-INS-i algorithm [79] and trimmed using trimAl v1.4.rev15 [80] with the -gt 0.8 option. Phylogenomic analysis was performed using IQ-TREE v.3.0.1 [81] with automatic model selection and branch support values estimated using Shimodaira–Hasegawa-like aLRT test. The resulting tree was visualized with Interactive Tree Of Life (iTOL) web server [82].

Immunofluorescence assay in *Toxoplasma gondii*

Toxoplasma gondii was cultured as described previously [10]. The sequence of TGGT1_224932 was synthesised with the addition of a 5' *EcoRI* restriction site and expression sequence, a 3' *NsiI* restriction site, as well as the remove of internal *NsiI* sites. This sequence was then inserted into the pTUB8mycGFPMyoATy expression vector [83]. The resulting plasmid was used to transfect

Toxoplasma which were then inoculated onto HFFs grown on glass coverslips. Cells were fixed with 4% paraformaldehyde after 1 day. An immunofluorescence assay was performed as described previously [10], using primary antibodies against Ty (1:800, anti-mouse,[84]) and TgTom40 (1:1,000, anti-rabbit,[42]), and imaged on a Nikon inverted AX/ AX-R Laser-Scanning Confocal Microscope using 63x objective. Z-stacking was performed on Nikon's NIS-Elements software using high-speed resonant scanner. The images were analysed using FIJI ImageJ X- 64 software [85].

Acknowledgements

We would like to thank Hannah Bridges and Judy Hirst (University of Cambridge) for the gift of bovine mitochondrial membrane. The help of Anzhelika Butenko (Institute of Parasitology, Biology Centre) with the phylogenetic analysis of ATPTG1 proteins is appreciated. We are grateful to Shikha Shikha (University of Glasgow) for discussion of the mitoribosomal subunits analysis. The authors gratefully acknowledge the Mass Spectrometry Facility, part of the MVLS Shared Research Facility and Laboratory of Mass Spectrometry at Biocev research center, Faculty of Science, Charles University, Prague, for their support & assistance in this work. This work was supported by Sir Henry Wellcome Fellowship (grant number 221681/Z/20/Z), Wellcome ISSF feasibility award (grant number 204820/Z/16/Z) and a Medical Research Council Career Development Award UKRI325 (grant reference: UKRI/MR/B000325/1) (to A. E. M); by the Czech Science Foundation grant 23-06479X (to J.L.) and by Wellcome Trust's Wellcome Investigator Award - 217173/Z/19/Z, and Wellcome Discovery Award - 310879/Z/24/Z (to L.S.).

References

1. Roger AJ, Muñoz-Gómez SA, Kamikawa R. The origin and diversification of mitochondria. Curr Biol. 2017;27: R1177–R1192. doi:10.1016/j.cub.2017.09.015

2. Hayward JA, van Dooren GG. Same same, but different: Uncovering unique features of the mitochondrial respiratory chain of apicomplexans. Mol Biochem Parasitol. 2019;232: 111204. doi:10.1016/j.molbiopara.2019.111204

3. Maclean AE, Hayward JA, Huet D, van Dooren GG, Sheiner L. The mystery of massive mitochondrial complexes: the apicomplexan respiratory chain. Trends Parasitol. 2022;38: 1041–1052. doi:10.1016/j.pt.2022.09.008

4. Waller RF, Carruthers VB. Adaptations and metabolic evolution of myzozoan protists across diverse lifestyles and environments. Microbiol Mol Biol Rev. 2024;88: e0019722. doi:10.1128/mmbr.00197-22

5. Flegontov P, Michálek J, Janouškovec J, Lai D-H, Jirků M, Hajdušková E, et al. Divergent mitochondrial respiratory chains in phototrophic relatives of apicomplexan parasites. Mol Biol Evol. 2015;32: 1115–31. doi:10.1093/molbev/msv021

6. Villalba A, Reece KS, Camino Ordás M, Casas SM, Figueras A. Perkinsosis in molluscs: A review. Aquat Living Resour. 2004;17: 411–432. doi:10.1051/alr:2004050

7. Mathur V, Wakeman KC, Keeling PJ. Parallel functional reduction in the mitochondria of apicomplexan parasites. Curr Biol. 2021;31: 2920-2928.e4. doi:10.1016/j.cub.2021.04.028

705 8. Salomaki ED, Terpis KX, Rueckert S, Kotyk M, Varadínová ZK, Čepička I, et al. Gregarine single-
706 cell transcriptomics reveals differential mitochondrial remodeling and adaptation in
707 apicomplexans. BMC Biol. 2021;19: 77. doi:10.1186/s12915-021-01007-2

708 9. MacLean AE, Shikha S, Ferreira Silva M, Gramelspacher MJ, Nilsen A, Liebman KM, et al.
709 Structure, assembly and inhibition of the *Toxoplasma gondii* respiratory chain supercomplex.
710 Nat Struct Mol Biol. 2025;32: 1424–1433. doi:10.1038/s41594-025-01531-7

711 10. Maclean AE, Bridges HR, Silva MF, Ding S, Ovciarikova J, Hirst J, et al. Complexome profile of
712 *Toxoplasma gondii* mitochondria identifies divergent subunits of respiratory chain complexes
713 including new subunits of cytochrome bc1 complex. PLoS Pathog. 2021;17: e1009301.
714 doi:10.1371/journal.ppat.1009301

715 11. Evers F, Cabrera-Orefice A, Elurbe DM, Kea-Te Lindert M, Boltryk SD, Voss TS, et al.
716 Composition and stage dynamics of mitochondrial complexes in *Plasmodium falciparum*. Nat
717 Commun. 2021;12: 3820. doi:10.1038/s41467-021-23919-x

718 12. Zwahlen SM, Hayward JA, Maguire CS, Qin AR, van Dooren GG. A myzozoan-specific protein is
719 an essential membrane-anchoring component of the succinate dehydrogenase complex in
720 *Toxoplasma* parasites. Open Biol. 2024;14: 230463. doi:10.1098/rsob.230463

721 13. Silva MF, Douglas K, Sandalli S, Maclean AE, Sheiner L. Functional and biochemical
722 characterization of the *Toxoplasma gondii* succinate dehydrogenase complex. PLoS Pathog.
723 2023;19: e1011867. doi:10.1371/journal.ppat.1011867

724 14. Hayward JA, Rajendran E, Zwahlen SM, Faou P, van Dooren GG. Divergent features of the
725 coenzyme Q:cytochrome *c* oxidoreductase complex in *Toxoplasma gondii* parasites. PLoS
726 Pathog. 2021;17: e1009211. doi:10.1371/journal.ppat.1009211

727 15. Seidi A, Muellner-Wong LS, Rajendran E, Tjhin ET, Dagley LF, Aw VY, et al. Elucidating the
728 mitochondrial proteome of *Toxoplasma gondii* reveals the presence of a divergent
729 cytochrome c oxidase. elife. 2018;7. doi:10.7554/eLife.38131

730 16. Matsubayashi M, Inaoka DK, Komatsuya K, Hatta T, Kawahara F, Sakamoto K, et al. novel
731 characteristics of mitochondrial electron transport chain from *Eimeria tenella*. Genes (Basel).
732 2019;10. doi:10.3390/genes10010029

733 17. Mühleip A, Kock Flygaard R, Ovciarikova J, Lacombe A, Fernandes P, Sheiner L, et al. ATP
734 synthase hexamer assemblies shape cristae of *Toxoplasma* mitochondria. Nat Commun.
735 2021;12: 120. doi:10.1038/s41467-020-20381-z

736 18. Huet D, Rajendran E, van Dooren GG, Lourido S. Identification of cryptic subunits from an
737 apicomplexan ATP synthase. Elife. 2018;7: e38097. doi:10.7554/eLife.38097

738 19. Salunke R, Mourier T, Banerjee M, Pain A, Shanmugam D. Highly diverged novel subunit
739 composition of apicomplexan F-type ATP synthase identified from *Toxoplasma gondii*. PLoS
740 Biol. 2018;16: e2006128. doi:10.1371/journal.pbio.2006128

741 20. Oborník M, Lukeš J. The organellar genomes of chromera and vitrella, the phototrophic
742 relatives of apicomplexan parasites. Annu Rev Microbiol. 2015;69: 129–44.
743 doi:10.1146/annurev-micro-091014-104449

744 21. Namasivayam S, Baptista RP, Xiao W, Hall EM, Doggett JS, Troell K, et al. A novel fragmented
745 mitochondrial genome in the protist pathogen *Toxoplasma gondii* and related tissue coccidia.
746 Genome Res. 2021;31: 852–865. doi:10.1101/gr.266403.120

747 22. Berná L, Rego N, Francia ME. The elusive mitochondrial genomes of apicomplexa: where are
748 we now? Front Microbiol. 2021;12: 751775. doi:10.3389/fmicb.2021.751775

749 23. Shikha S, Tobiasson V, Ferreira Silva M, Ovciarikova J, Beraldi D, Mühleip A, et al. Numerous
750 rRNA molecules form the apicomplexan mitoribosome via repurposed protein and RNA
751 elements. Nat Commun. 2025;16: 817. doi:10.1038/s41467-025-56057-9

752 24. Wang C, Kassem S, Rocha REO, Sun P, Nguyen T-T, Kloehn J, et al. Apicomplexan mitoribosome
753 from highly fragmented rRNAs to a functional machine. Nat Commun. 2024;15: 10689.
754 doi:10.1038/s41467-024-55033-z

755 25. Gornik SG, Flores V, Reinhardt F, Erber L, Salas-Leiva DE, Douvropoulou O, et al. mitochondrial
756 genomes in *Perkinsus* Decode Conserved Frameshifts in All Genes. Mol Biol Evol.
757 2022;39(10):msac191. doi:10.1093/molbev/msac191

758 26. Einarsson E, Lassadi I, Zielinski J, Guan Q, Wyler T, Pain A, et al. Development of the myzozoan
759 aquatic parasite *Perkinsus marinus* as a versatile experimental genetic model organism.
760 Protist. 2021;172: 125830. doi:10.1016/j.protis.2021.125830

761 27. Heide H, Bleier L, Steger M, Ackermann J, Dröse S, Schwamb B, et al. Complexome profiling
762 identifies TMEM126B as a component of the mitochondrial complex I assembly complex. Cell
763 Metab. 2012;16: 538–49. doi:10.1016/j.cmet.2012.08.009

764 28. Cabrera-Orefice A, Potter A, Evers F, Hevler JF, Guerrero-Castillo S. Complexome Profiling-
765 Exploring Mitochondrial Protein Complexes in Health and Disease. Front Cell Dev Biol. 2021;9:
766 796128. doi:10.3389/fcell.2021.796128

767 29. Wittig I, Malacarne PF. Complexome Profiling: Assembly and Remodeling of Protein
768 Complexes. Int J Mol Sci. 2021;22. doi:10.3390/ijms22157809

769 30. Nina PB, Morrisey JM, Ganesan SM, Ke H, Pershing AM, Mather MW, et al. ATP synthase
770 complex of *Plasmodium falciparum*: dimeric assembly in mitochondrial membranes and
771 resistance to genetic disruption. J Biol Chem. 2011;286: 41312–41322.
772 doi:10.1074/jbc.M111.290973

773 31. Fernández-Robledo JA, Lin Z, Vasta GR. Transfection of the protozoan parasite *Perkinsus*
774 *marinus*. Mol Biochem Parasitol. 2008;157: 44–53. doi:10.1016/j.molbiopara.2007.09.007

775 32. Schröder L, Eubel H, Braun H-P. Complexome profiling of plant mitochondrial fractions.
776 Methods Mol Biol. 2022;2363: 101–110. doi:10.1007/978-1-0716-1653-6_9

777 33. Giese H, Meisterknecht J, Heidler J, Wittig I. Mitochondrial Complexome Profiling. Methods
778 Mol Biol. 2021;2192: 269–285. doi:10.1007/978-1-0716-0834-0_19

779 34. Barylyuk K, Koreny L, Ke H, Butterworth S, Crook OM, Lassadi I, et al. A comprehensive
780 subcellular atlas of the *Toxoplasma p*roteome via hyperLOPIT provides spatial context for
781 protein functions. Cell Host Microbe. 2020;28: 752-766.e9. doi:10.1016/j.chom.2020.09.011

35. van Esveld SL, Meerstein-Kessel L, Boshoven C, Baaij JF, Barylyuk K, Coolen JPM, et al. A Prioritized and Validated Resource of Mitochondrial Proteins in Plasmodium Identifies Unique Biology. mSphere. 2021;6: e0061421. doi:10.1128/mSphere.00614-21

36. Schikowsky C, Senkler J, Braun H-P. SDH6 and SDH7 contribute to anchoring succinate dehydrogenase to the inner mitochondrial membrane in *Arabidopsis thaliana*. Plant Physiol. 2017;173: 1094–1108. doi:10.1104/pp.16.01675

37. Morales J, Mogi T, Mineki S, Takashima E, Mineki R, Hirawake H, et al. Novel mitochondrial complex II isolated from *Trypanosoma cruzi* is composed of 12 peptides including a heterodimeric Ip subunit. J Biol Chem. 2009;284: 7255–63. doi:10.1074/jbc.M806623200

38. Mühleip A, Flygaard RK, Baradaran R, Haapanen O, Gruhl T, Tobiasson V, et al. Structural basis of mitochondrial membrane bending by the I-II-III2-IV2 supercomplex. Nature. 2023;615: 934–938. doi:10.1038/s41586-023-05817-y

39. Wú F, Mühleip A, Gruhl T, Sheiner L, Maréchal A, Amunts A. Structure of the II2-III2-IV2 mitochondrial supercomplex from the parasite *Perkinsus marinus*. 2024. bioXiv. doi:10.1101/2024.05.25.595893

40. Signes A, Fernandez-Vizarra E. Assembly of mammalian oxidative phosphorylation complexes I-V and supercomplexes. Essays Biochem. 2018;62: 255–270. doi:10.1042/EBC20170098

41. Ovciarikova J, Lemgruber L, Stilger KL, Sullivan WJ, Sheiner L. Mitochondrial behaviour throughout the lytic cycle of *Toxoplasma gondii*. Sci Rep. 2017;7: 42746. doi:10.1038/srep42746

42. van Dooren GG, Yeoh LM, Striepen B, McFadden GI. The import of proteins into the mitochondrion of *Toxoplasma gondii*. Journal of Biological Chemistry. 2016;291: 19335–19350. doi:10.1074/jbc.M116.725069

43. Usey MM, Huet D. ATP synthase-associated coiled-coil-helix-coiled-coil-helix (CHCH) domain-containing proteins are critical for mitochondrial function in Toxoplasma gondii. mBio. 2023;14: e0176923. doi:10.1128/mbio.01769-23

44. García-Guerrero AE, Marvin RG, Blackwell AM, Sigala PA. Biogenesis of cytochromes c and c1 in the electron transport chain of malaria parasites. ACS Infect Dis. 2025;11: 813–826. doi:10.1021/acsinfecdis.4c00450

45. Waller RF, Jackson CJ. Dinoflagellate mitochondrial genomes: stretching the rules of molecular biology. Bioessays. 2009;31: 237–45. doi:10.1002/bies.200800164

46. Desai N, Brown A, Amunts A, Ramakrishnan V. The structure of the yeast mitochondrial ribosome. Science. 2017;355: 528–531. doi:10.1126/science.aal2415

47. Amunts A, Brown A, Toots J, Scheres SHW, Ramakrishnan V. Ribosome. The structure of the human mitochondrial ribosome. Science. 2015;348: 95–98. doi:10.1126/science.aaa1193

48. Jeninga MD, Quinn JE, Petter M. ApiAP2 transcription factors in apicomplexan parasites. Pathogens. 2019;8. doi:10.3390/pathogens8020047

49. Oberstaller J, Pumpalova Y, Schieler A, Llinás M, Kissinger JC. The *Cryptosporidium parvum* ApiAP2 gene family: insights into the evolution of apicomplexan AP2 regulatory systems. Nucleic Acids Res. 2014;42: 8271–84. doi:10.1093/nar/gku500

822 50. Huang X, Luan B, Wu J, Shi Y. An atomic structure of the human 26S proteasome. Nat Struct
823 Mol Biol. 2016;23: 778–85. doi:10.1038/nsmb.3273

824 51. Zhu Q, Zhu X, Zhang L. ER membrane complex (EMC): Structure, functions, and roles in
825 diseases. FASEB J. 2024;38: e23539. doi:10.1096/fj.202302266R

826 52. Hammond M, Dorrell RG, Speijer D, Lukeš J. Eukaryotic cellular intricacies shape
827 mitochondrial proteomic complexity. Bioessays. 2022;44: e2100258.
828 doi:10.1002/bies.202100258

829 53. Hammond MJ, Nenarokova A, Butenko A, Zoltner M, Dobáková EL, Field MC, et al. A uniquely
830 complex mitochondrial proteome from *Euglena gracilis*. Mol Biol Evol. 2020;37: 2173–2191.
831 doi:10.1093/molbev/msaa061

832 54. Santos HJ, Makiuchi T, Nozaki T. Reinventing an organelle: the reduced mitochondrion in
833 parasitic protists. Trends Parasitol. 2018;34: 1038–1055. doi:10.1016/j.pt.2018.08.008

834 55. Karnkowska A, Vacek V, Zubáčová Z, Treitli SC, Petrželková R, Eme L, et al. A Eukaryote without
835 a Mitochondrial Organelle. Curr Biol. 2016;26: 1274–84. doi:10.1016/j.cub.2016.03.053

836 56. Bartošová-Sojková P, Butenko A, Richtová J, Fiala I, Oborník M, Lukeš J. Inside the Host:
837 Understanding the Evolutionary Trajectories of Intracellular Parasitism. Annu Rev Microbiol.
838 2024;78: 39–59. doi:10.1146/annurev-micro-041222-025305

839 57. Albalat R, Cañestro C. Evolution by gene loss. Nat Rev Genet. 2016;17: 379–91.
840 doi:10.1038/nrg.2016.39

841 58. Zíková A, Hampl V, Paris Z, Týč J, Lukeš J. Aerobic mitochondria of parasitic protists: diverse
842 genomes and complex functions. Mol Biochem Parasitol. 2016;209: 46–57.
843 doi:10.1016/j.molbiopara.2016.02.007

844 59. Zhou L, Maldonado M, Padavannil A, Guo F, Letts JA. Structures of *Tetrahymena*'s respiratory
845 chain reveal the diversity of eukaryotic core metabolism. Science. 2022;376: 831–839.
846 doi:10.1126/science.abn7747

847 60. Han F, Hu Y, Wu M, He Z, Tian H, Zhou L. Structures of *Tetrahymena thermophila* respiratory
848 megacomplexes on the tubular mitochondrial cristae. Nat Commun. 2023;14: 2542.
849 doi:10.1038/s41467-023-38158-5

850 61. Flygaard RK, Mühleip A, Tobiasson V, Amunts A. Type III ATP synthase is a symmetry-deviated
851 dimer that induces membrane curvature through tetramerization. Nat Commun. 2020;11:
852 5342. doi:10.1038/s41467-020-18993-6

853 62. Waller RF, Keeling PJ, van Dooren GG, McFadden GI. Comment on "A green algal apicoplast
854 ancestor". Science. 2003;301: 49; author reply 49. doi:10.1126/science.1084684

855 63. Huynen MA, Elurbe DM. Mitochondrial complex complexification. Science. 2022;376: 794–
856 795. doi:10.1126/science.abq0368

857 64. Waltz F, Salinas-Giegé T, Englmeier R, Meichel H, Soufari H, Kuhn L, et al. How to build a
858 ribosome from RNA fragments in *Chlamydomonas* mitochondria. Nat Commun. 2021;12:
859 7176. doi:10.1038/s41467-021-27200-z

65. Ramrath DJF, Niemann M, Leibundgut M, Bieri P, Prange C, Horn EK, et al. Evolutionary shift toward protein-based architecture in trypanosomal mitochondrial ribosomes. Science. 2018;362. doi:10.1126/science.aau7735

66. Vaidya AB, Mather MW. Mitochondrial evolution and functions in malaria parasites. Annu Rev Microbiol. 2009;63: 249–67. doi:10.1146/annurev.micro.091208.073424

67. Alston CL, Compton AG, Formosa LE, Strecker V, Oláhová M, Haack TB, et al. Biallelic mutations in TMEM126B cause severe complex I deficiency with a variable clinical phenotype. Am J Hum Genet. 2016;99: 217–27. doi:10.1016/j.ajhg.2016.05.021

68. Guerrero-Castillo S, Baertling F, Kownatzki D, Wessels HJ, Arnold S, Brandt U, et al. The assembly pathway of mitochondrial respiratory chain complex I. Cell Metab. 2017;25: 128–139. doi:10.1016/j.cmet.2016.09.002

69. Flores-Mireles D, Camacho-Villasana Y, Lutikurti M, García-Guerrero AE, Lozano-Rosas G, Chagoya V, et al. The cytochrome b carboxyl terminal region is necessary for mitochondrial complex III assembly. Life Sci Alliance. 2023;6. doi:10.26508/lsa.202201858

70. Röhricht H, Schwartzmann J, Meyer EH. Complexome profiling reveals novel insights into the composition and assembly of the mitochondrial ATP synthase of *Arabidopsis thaliana*. Biochim Biophys Acta Bioenerg. 2021;1862: 148425. doi:10.1016/j.bbabio.2021.148425

71. Lang J, König K, Venn B, Zeilfelder S, Ostermeier M, Spaniol B, et al. Complexome profiling of the *Chlamydomonas* psb28 mutant reveals TEF5 as an early PSII assembly factor. Plant Cell. 2025;37. doi:10.1093/plcell/koaf055

72. Castañeda-Tamez P, Chiquete-Félix N, Uribe-Carvajal S, Cabrera-Orefice A. The mitochondrial respiratory chain from *Rhodotorula mucilaginosa*, an extremophile yeast. Biochim Biophys Acta Bioenerg. 2024;1865: 149035. doi:10.1016/j.bbabio.2024.149035

73. Sabar M, Balk J, Leaver CJ. Histochemical staining and quantification of plant mitochondrial respiratory chain complexes using blue-native polyacrylamide gel electrophoresis. Plant J. 2005;44: 893–901. doi:10.1111/j.1365-313X.2005.02577.x

74. Rappsilber J, Mann M, Ishihama Y. Protocol for micro-purification, enrichment, pre-fractionation and storage of peptides for proteomics using StageTips. Nat Protoc. 2007;2: 1896–1906. doi:10.1038/nprot.2007.261

75. Cox J, Mann M. MaxQuant enables high peptide identification rates, individualized p.p.b.-range mass accuracies and proteome-wide protein quantification. Nat Biotechnol. 2008;26: 1367–72. doi:10.1038/nbt.1511

76. Abueg LAL, Afgan E, Allart O, Awan AH, Bacon WA, Baker D, et al. The Galaxy platform for accessible, reproducible, and collaborative data analyses: 2024 update. Nucleic Acids Res. 2024;52: W83–W94. doi:10.1093/nar/gkae410

77. Giese H, Ackermann J, Heide H, Bleier L, Dröse S, Wittig I, et al. NOVA: a software to analyze complexome profiling data. Bioinformatics. 2015;31: 440–1. doi:10.1093/bioinformatics/btu623

78. Sobala ŁF. LukProt: A database of eukaryotic predicted proteins designed for investigations of animal origins. Genome Biol Evol. 2024;16. doi:10.1093/gbe/evae231

79. Katoh K, Standley DM. MAFFT multiple sequence alignment software version 7: improvements in performance and usability. Mol Biol Evol. 2013;30: 772–80. doi:10.1093/molbev/mst010

80. Capella-Gutiérrez S, Silla-Martínez JM, Gabaldón T. trimAl: a tool for automated alignment trimming in large-scale phylogenetic analyses. Bioinformatics. 2009;25: 1972–3. doi:10.1093/bioinformatics/btp348

81. Wong T, Ly-Trong N, Ren H, Baños H, Roger A, Susko E, et al. IQ-TREE 3: phylogenomic inference software using complex evolutionary models. 2025. doi:10.32942/X2P62N

82. Letunic I, Bork P. Interactive Tree of Life (iTOL) v6: recent updates to the phylogenetic tree display and annotation tool. Nucleic Acids Res. 2024;52: W78–W82. doi:10.1093/nar/gkae268

83. Herm-Gotz A. *Toxoplasma gondii* myosin A and its light chain: a fast, single-headed, plus-end-directed motor. EMBO J. 2002;21: 2149–2158. doi:10.1093/emboj/21.9.2149

84. Bastin P, Bagherzadeh A, Matthews KR, Gull K. A novel epitope tag system to study protein targeting and organelle biogenesis in *Trypanosoma brucei*. Mol Biochem Parasitol. 1996;77: 235–239. doi:10.1016/0166-6851(96)02598-4

85. Schindelin J, Arganda-Carreras I, Frise E, Kaynig V, Longair M, Pietzsch T, et al. Fiji: an open-source platform for biological-image analysis. Nat Methods. 2012;9: 676–682. doi:10.1038/nmeth.2019

86. Meng EC, Goddard TD, Pettersen EF, Couch GS, Pearson ZJ, Morris JH, et al. UCSF ChimeraX: Tools for structure building and analysis. Protein Sci. 2023;32: e4792. doi:10.1002/pro.4792

87. Abramson J, Adler J, Dunger J, Evans R, Green T, Pritzel A, et al. Accurate structure prediction of biomolecular interactions with AlphaFold 3. Nature. 2024;630: 493–500. doi:10.1038/s41586-024-07487-w

88. Waterhouse AM, Procter JB, Martin DMA, Clamp M, Barton GJ. Jalview Version 2—a multiple sequence alignment editor and analysis workbench. Bioinformatics. 2009;25: 1189–1191. doi:10.1093/bioinformatics/btp033

928 **Main figures**

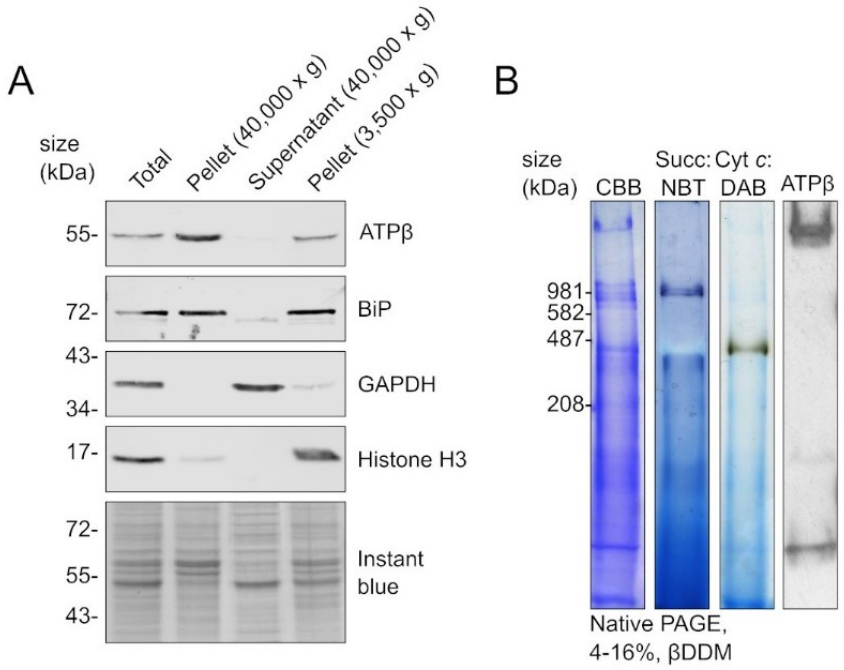

929

930 **Figure 1: Isolation of mitochondrially-enriched fractions**
931 (A) Immunoblot analysis of total cell lysate (Total) and purification fractions using antibodies against
932 marker proteins of various cell compartments. The pellet from the 3,500 x *g* centrifugation step
933 contains unbroken cells and heavy cell components, from the 40,000 x *g* step the supernatant contains
934 soluble cytosolic proteins, and the pellet mitochondrial and organellar material. 7.5 µg of protein was
935 loaded per lane with equal loading confirmed by instant blue staining (bottom panel). The following
936 antibodies were used: ATPβ (mitochondrion), BiP (ER), GAPDH (cytosol) and Histone H3 (nucleus). (B)
937 Blue-native PAGE analysis of mitochondrially-enriched material treated with βDDM and separated on
938 a 4-16% Bis-Tris gel. Total protein was visualized by Coomassie staining, complex II activity by an in-gel
939 succinate: nitroblue tetrazolium (NBT) activity stain, complex IV activity by an in-gel cyt *c*: 3,3'-
940 Diaminobenzidine (DAB) activity stain and ATP synthase by immunoblot analysis using the anti-ATPβ
941 antibody.

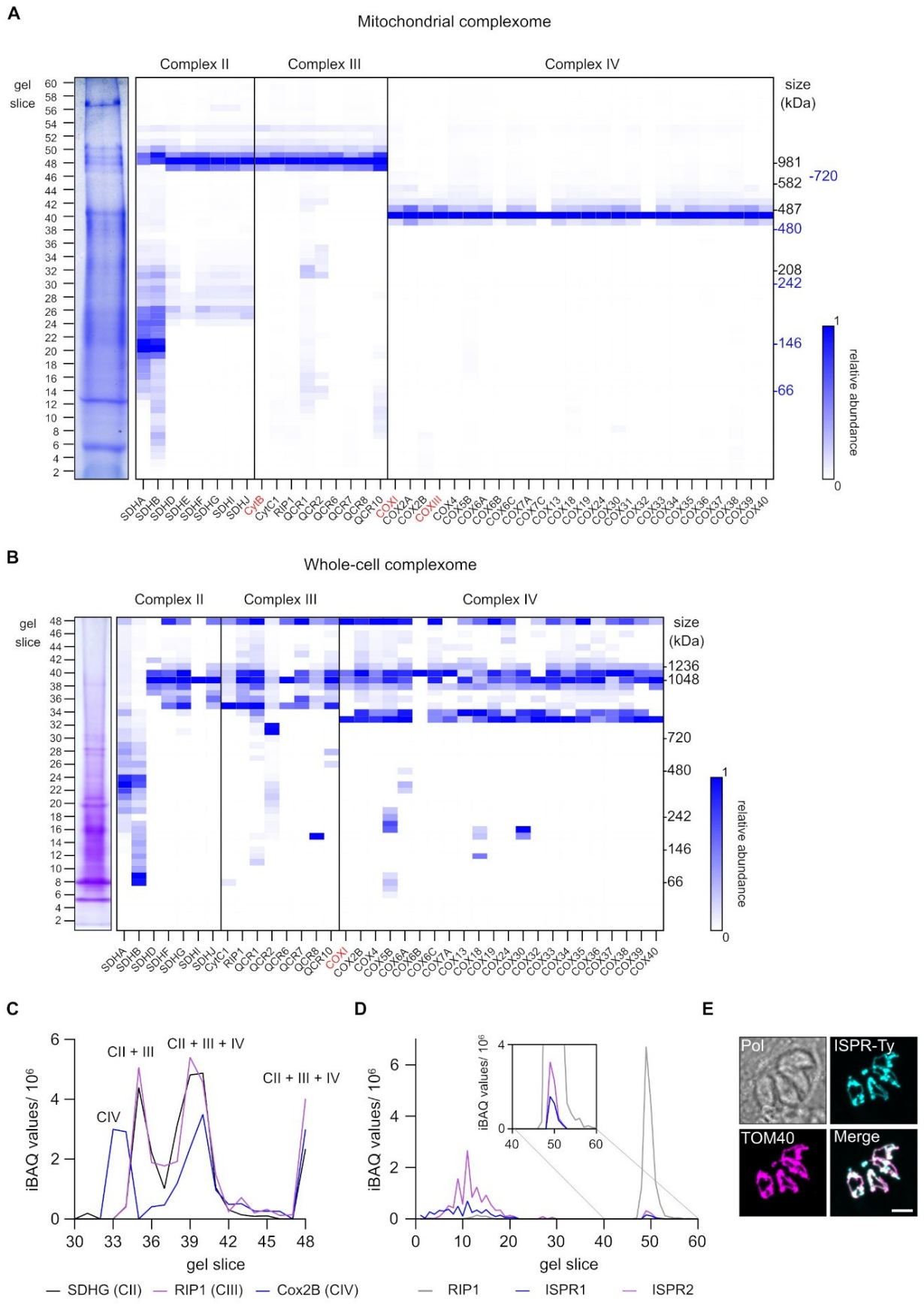
A
Mitochondrial complexome
Complex II
Complex III
Complex IV
gel slice
size (kDa)
981
582
487
208
146
66
720
480
242
relative abundance
SDHA SDHB SDHD SDHE SDHF SDHG SDHI SDHJ CytB CytC1 RIP1 QCR1 QCR2 QCR6 QCR7 QCR8 QCR10 COXI COX2A COX2B COXIII COX4 COX5B COX6A COX6B COX6C COX7A COX7C COX13 COX18 COX19 COX24 COX30 COX31 COX32 COX33 COX34 COX35 COX36 COX37 COX38 COX39 COX40
B
Whole-cell complexome
Complex II
Complex III
Complex IV
gel slice
size (kDa)
1236
1048
720
480
242
146
66
relative abundance
C
iBAQ values/ 10^6
CII + III
CII + III + IV
CIV
CII + III + IV
gel slice
SDHG (CII)
RIP1 (CIII)
Cox2B (CIV)
D
iBAQ values/ 10^6
gel slice
RIP1
ISPR1
ISPR2
E
Pol
ISPR-Ty
TOM40
Merge

942

943 **Figure 2: Complexome profiles of mETC complexes**
944 (A) Heatmaps of the complexome profiles from mitochondrially-enriched material of mETC complex
945 subunits from complex II, complex III and complex IV. Each row represents a gel slice, with the gel slice
946 number indicated on the left and the molecular weight, based on the migration of mammalian
947 mitochondrial complexes (black) and soluble proteins (blue), on the right. Subunit IDs are shown at
948 the bottom of their corresponding profile, with mitochondrially-encoded subunits highlighted in red.
949 Dark blue indicates the highest relative abundance (1) and white the lowest (0). Coomassie-stained
950 Native PAGE gel on which the analysis was performed is depicted on the left of the profile. Data shown
951 is from replicate 1. (B) Heatmap of the whole-cell complexome of mETC complexes, as in part *(A)*.
952 Molecular weight, based on the migration of soluble proteins on the right is shown on the right. (C)
953 Abundance profile of complex II subunit SDHG, complex III subunit RIP1 and complex IV subunit Cox2B
954 across all gel slices. Protein abundance is displayed as iBAQ values. Data shown is from whole-cell
955 complexome. (D) Abundance profile of ISPR1, ISPR2 and complex III subunit RIP1 across all slices.
956 Protein abundance is displayed as iBAQ values. Data shown is from replicate 2. (E)
957 Immunofluorescence assay of *Toxoplasma gondii* transiently expressing a Ty-epitope tagged version of
958 *Tg*ISPR. Samples labelled with anti-Ty to detect *Tg*ISPR-Ty (cyan) and anti-Tom40 (magenta) to detect
959 the mitochondrial marker protein Tom40. Scale bar is 5 µM.

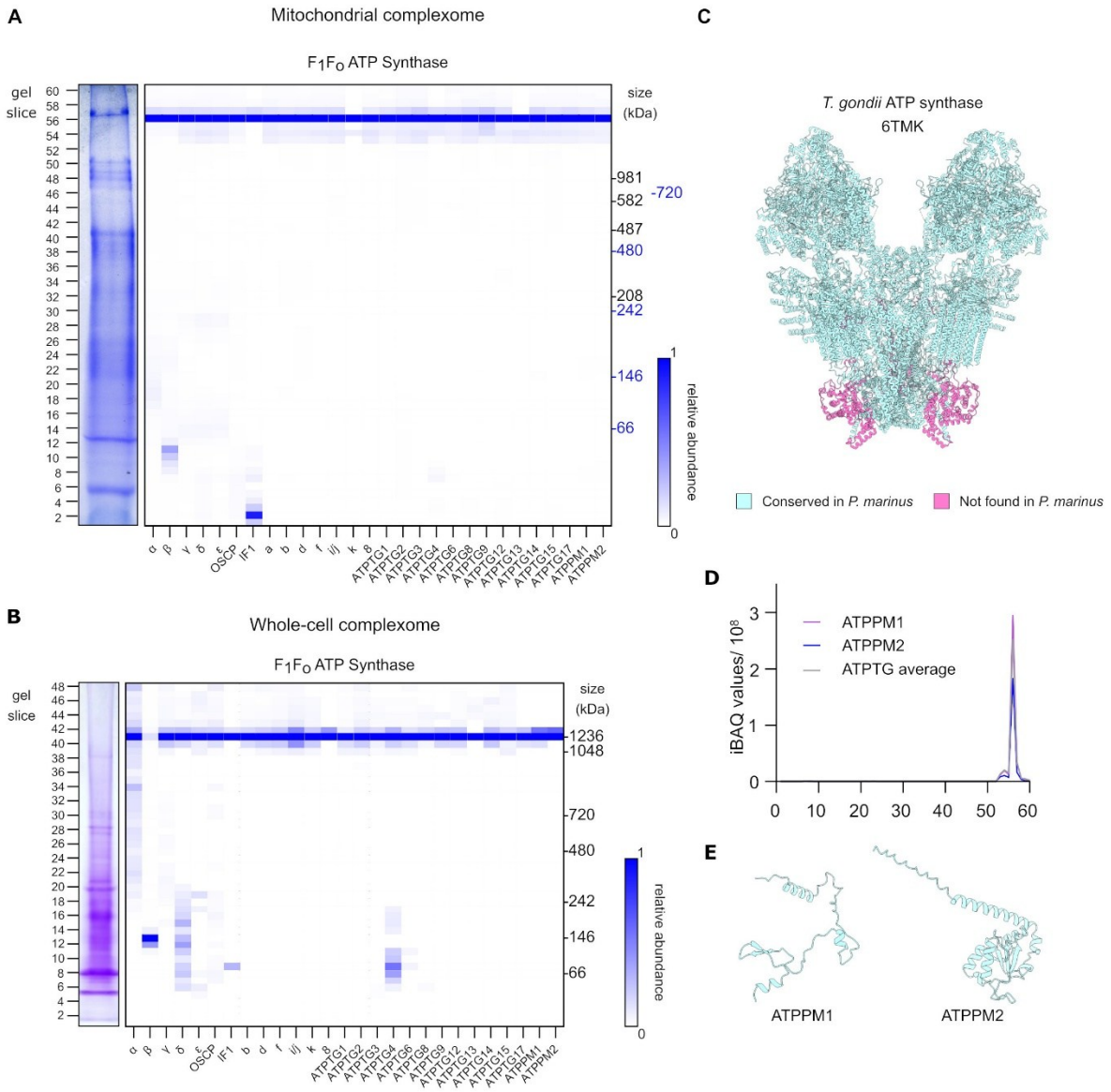

Figure 3: Complexome profiles of the F_1F_o ATP synthase complex

(A) Heatmap of the complexome profile from mitochondrially-enriched material of ATP synthase. Each row represents a gel slice, with the gel slice number indicated on the left and the molecular weight, based on the migration of mammalian mitochondrial complexes (black) and soluble proteins (blue), on the right. Subunit IDs are shown at the bottom of their corresponding profile. Dark blue indicates the highest relative abundance (1) and white the lowest (0). Coomassie-stained Native PAGE gel on which the analysis was performed is depicted on the left of the profile. Data shown is from replicate 1. (B) Heatmap of the whole-cell complexome of ATP synthase, as in part *(A)*. Molecular weight, based on the migration of soluble proteins on the right is shown on the right. (C) Structure of ATP Synthase dimer from *Toxoplasma gondii* (PDB 6TMK, [17]) with subunits conserved in *Perkinsus* coloured blue, and subunit not found in coloured pink. Visualised using ChimeraX [86]. (D) Abundance profile of ATPPM1, ATPPM2, and the average abundance of all ATPTG subunits across all gel slices. Protein abundance is displayed as iBAQ values. Data shown is from replicate 1. (E) Structural prediction of ATPPM1 and ATPPM2 (predicted using Alphafold3 [87]).

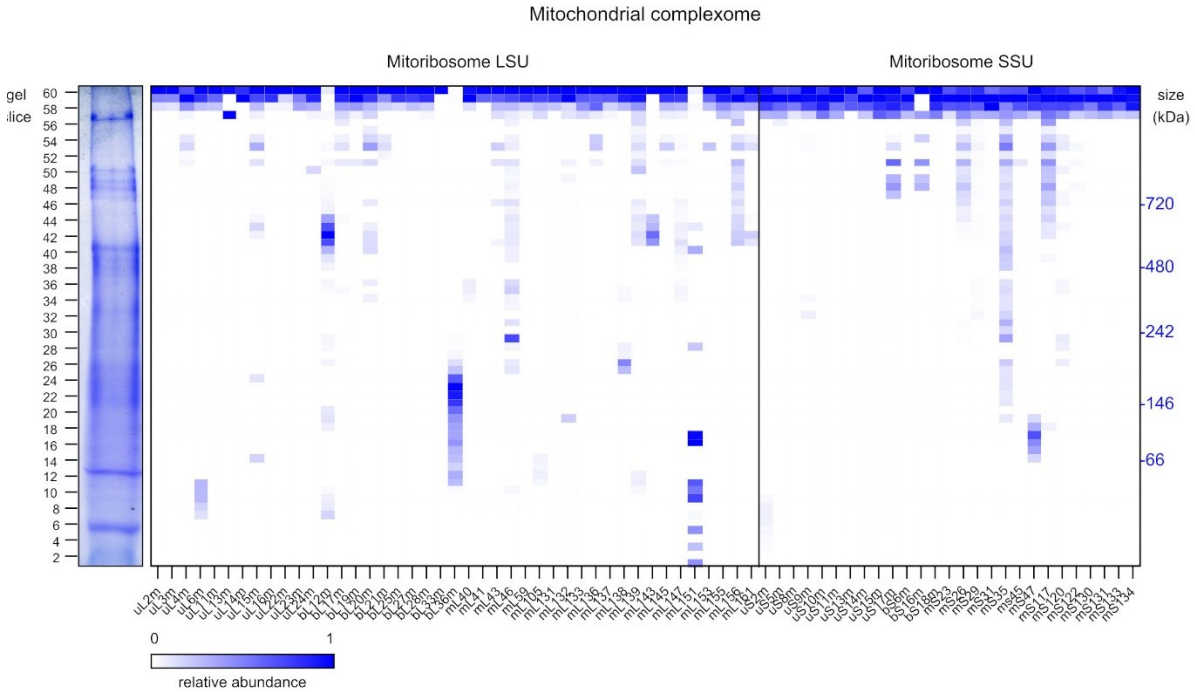

975

976 **Figure 4: Complexome profile of mitoribosome**

977 Heatmap of the complexome profile of the mitochondrial ribosome, showing subunits of the LSU and
978 SSU. Each row represents a gel slice, with the gel slice number indicated on the left and the molecular
979 weight, based on the migration of mammalian mitochondrial complexes (black) and soluble proteins
980 (blue), on the right. Subunit IDs are shown at the bottom of their corresponding profile. Dark blue
981 indicates the highest relative abundance (1) and white the lowest (0). Coomassie-stained Native PAGE
982 gel on which the analysis was performed is depicted on the left of the profile. Data shown is from
983 replicate 1.

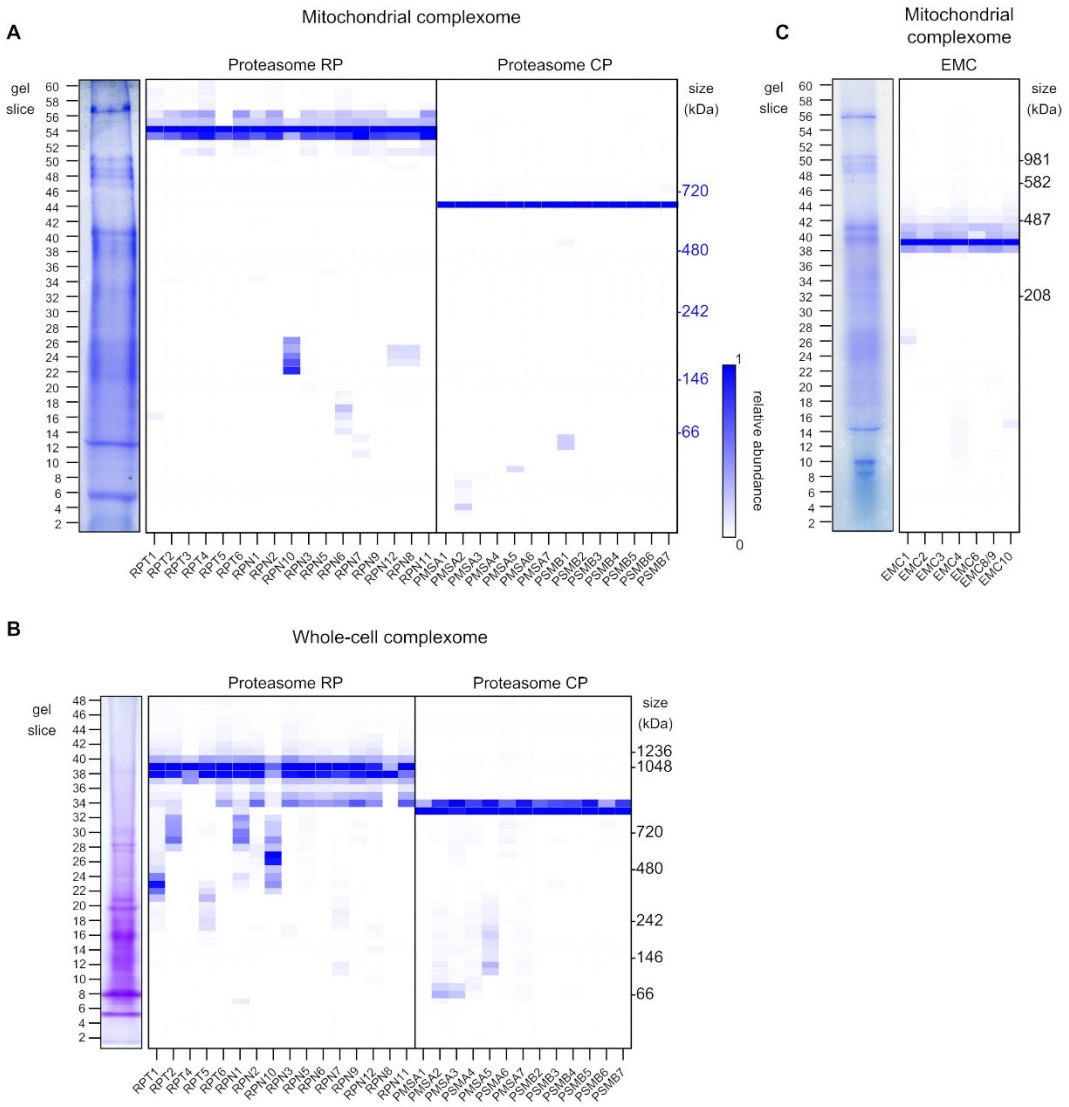

Figure 5: Complexome profile of non-mitochondrial complexes

(A) Heatmap of the complexome profile from mitochondrially-enriched material of the 26S proteasome, comprised of the 19S regulatory particle (RP) and the 20S core particle (CP). Each row represents a gel slice, with the gel slice number indicated on the left and the molecular weight, based on the migration of soluble proteins (blue), on the right. Subunit IDs are shown at the bottom of their corresponding profile. Dark blue indicates the highest relative abundance (1) and white the lowest (0). Coomassie-stained Native PAGE gel on which the analysis was performed is depicted on the left of the profile. Data shown is from replicate 1. (B) Heatmap of the whole-cell complexome of the 26S proteasome, comprised of the 19S regulatory particle (RP) and the 20S core particle (CP), as in part *(A)*. Molecular weight, based on the migration of soluble proteins on the right is shown on the right. (C) Heatmap of the complexome profile from mitochondrially-enriched material of the Endoplasmic reticulum membrane protein complex (EMC), as in part *(A)*. Molecular weight is based on the migration of mammalian mitochondrial complexes. Data shown is from replicate 2.

Supplemental Figures

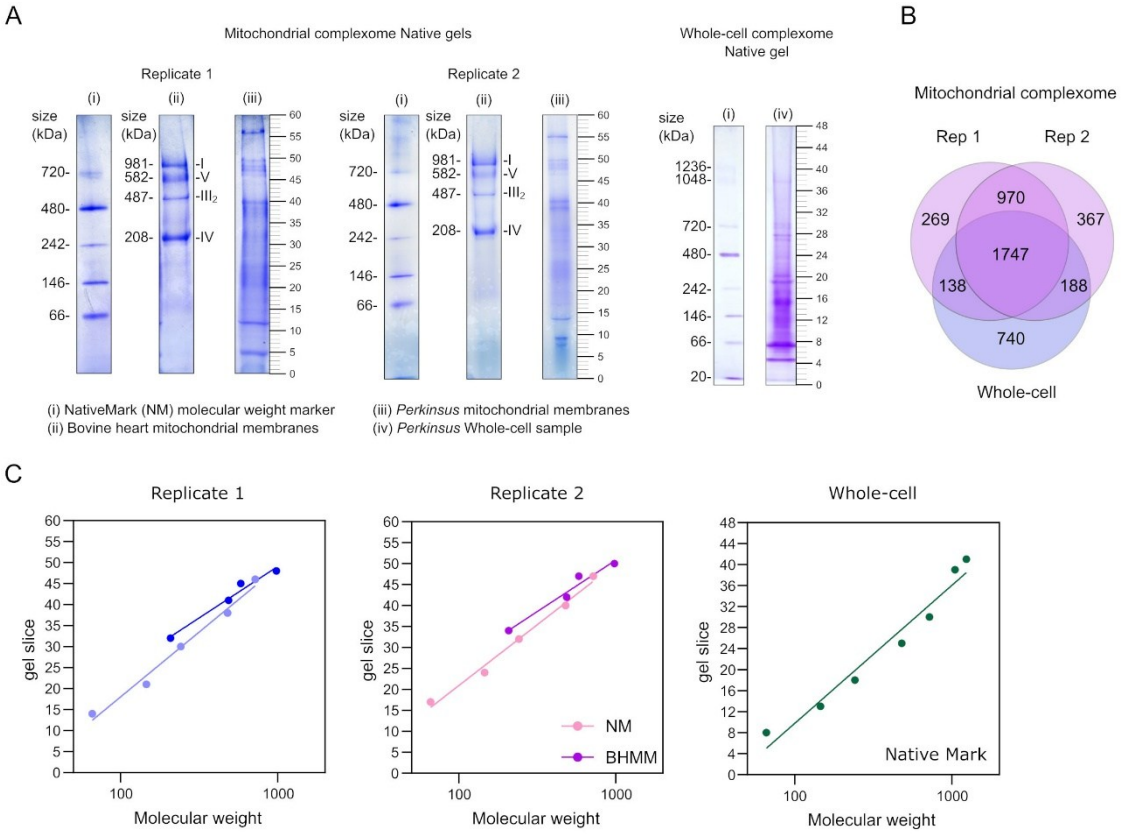

Figure S1: Generating complexome profiles

(A) Coomassie-stained Native PAGE gels showing molecular weight markers (i- NativeMark, ii- Bovine mitochondrial membranes), *Perkinsus* mitochondrially-enriched material (iii) and *Perkinsus* whole-cell material (iv) used in generating the complexome. Molecular weight markers and *Perkinsus* material were run on the same gel and aligned, with corresponding gel slices numbers (1-60) shown on the right-hand side. For the mitochondrially-enriched material, gels from both replicate 1 and 2 are shown. (B) Comparison of proteins identified in each repetition of the mitochondrial and the whole-cell samples. (C) Mass calibration analysis using NativeMark and Bovine mitochondrial membrane molecular weight markers. Molecular weight and corresponding gel slice were plotted and a non-linear regression, semi-log line plotted. Full details of mass calibration are in Table S3.

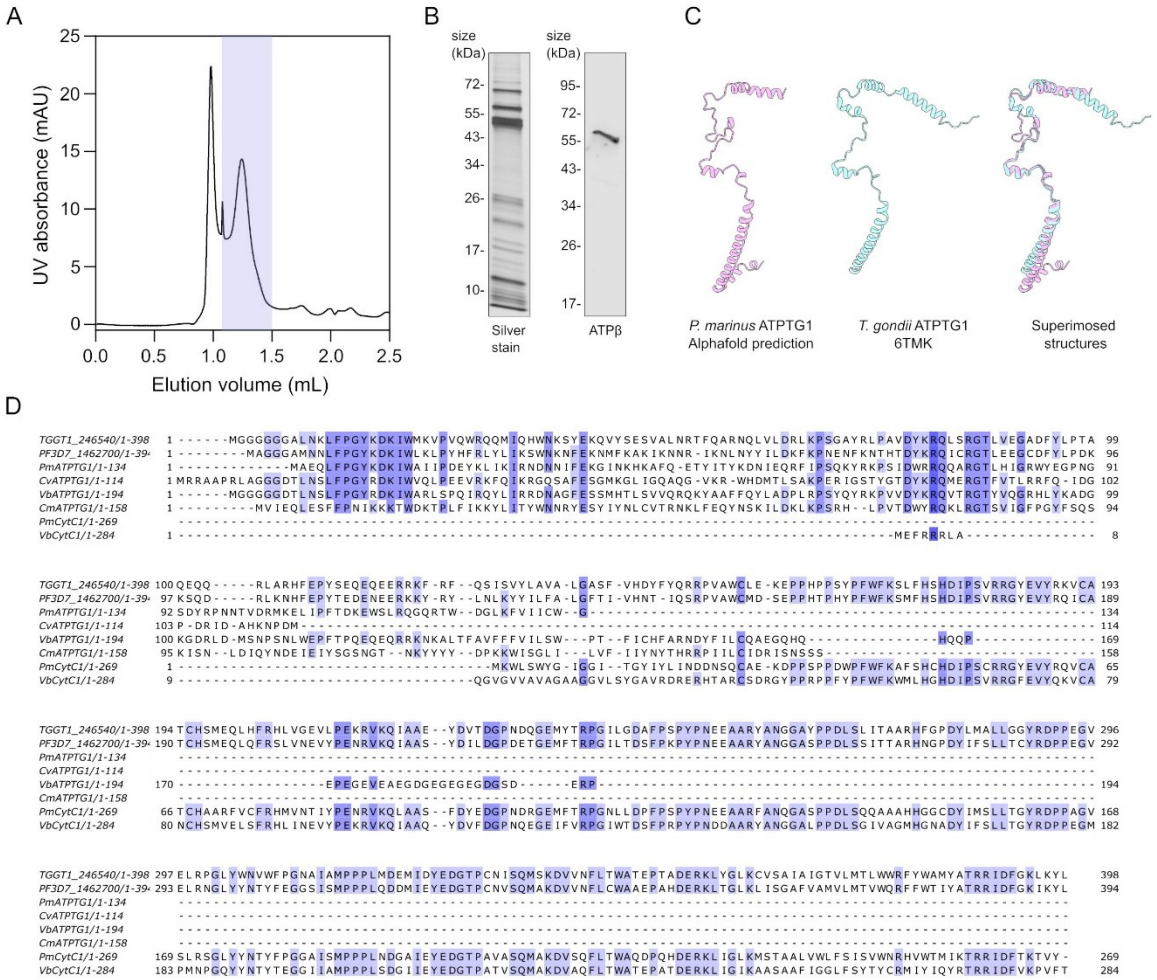

Figure S2: Analysis of ATP synthase subunit ATPTG1

(A) Chromatogram displaying UV 1_280 of gel filtration of purified ATP synthase using a Superose 6 increase 3.2/300 column. Left-most peak represents void-volume. The fractions highlighted in blue were combined and concentrated using a 100 MWCO spin concentrator before analysis via immunoblot and mass spectrometry. (B) SDS-PAGE analysis of purified ATP synthase. Gel was either silver stained to visualize protein subunits or subjected to immunoblot analysis with the ATPβ antibody. (C) Structural prediction of *P. marinus* ATPTG1 (predicted using Alphafold3 [87]) (left), the structure of *T. gondii* ATPTG1 (PDB 6TMK; [17]) (center) and the superimposition of the two structures (RMSD = 1.122 Å) (right). Visualized using ChimeraX [86]. (D) Alignment of ATPTG1, CytC1 and fusion proteins from across the myzozoa. ATPTG1 proteins: *Perkinsus marinus* Pmar_PMAR013021; *Chromera velia* Cvel_13300*; Vitrella brassicaformis Vbra_20035*; *Cryptosporidium muris* CMU_009920. CytC1 proteins: *Perkinsus marinus* Pmar_PMAR028703; *Vitrella brassicaformis* Vbra_21749. Fusion proteins: TGGT1_246540 from *Toxoplasma gondii*; PF3D7_1462700 from *Plasmodium falciparum*. Alignments were made using Clustal Omega and visualized using JalView (v10.0.7) [88]. Colour coding depicts percent identity.

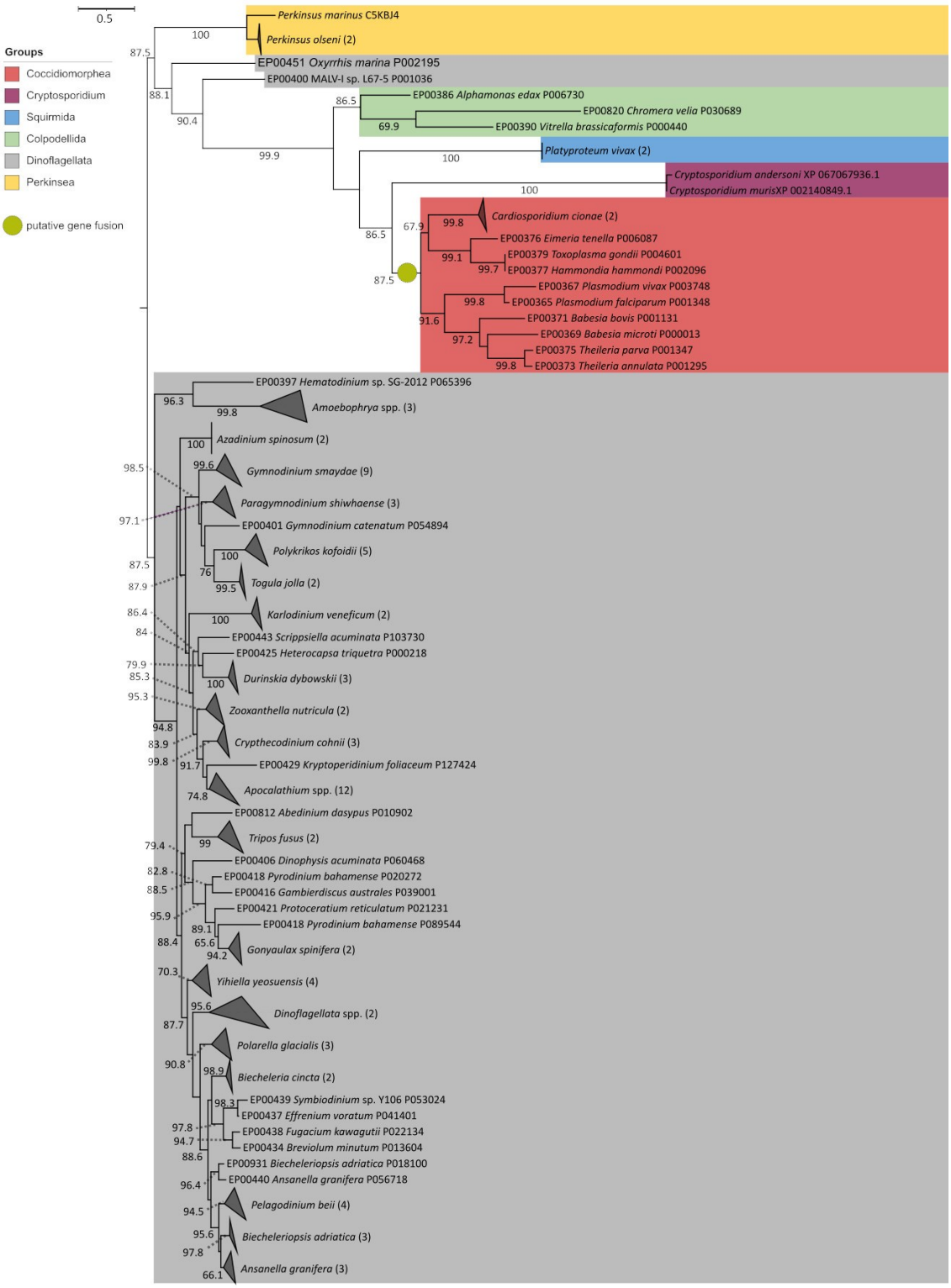

Figure S3: Phylogeny of ATPTG1 homologues from various myzozoans.
A maximum-likelihood phylogenetic tree inferred with IQ-TREE v.3.0.1 on the trimmed protein alignment containing 170 amino acid positions. The tree was inferred with the LG+I+G4 model automatically selected according to Bayesian information criterion. Branch support values represent Shimodaira–Hasegawa-like aLRT (SH-aLRT) test scores; only values ≥60 are shown. The horizontal bar indicates number of substitutions per site.

1033 ## Supplementary tables

1034

1035 **Table S1**: Complexome datasets from mitochondrially enriched material, replicates 1 and 2.
1036 Abundance information is displayed as iBAQ values.
1037 **Table S2**: Complexome datasets from whole-cell material. Abundance information is displayed as iBAQ
1038 values.
1039 **Table S3**: Mass calibration – calculation of apparent mass found in each gel slice based on the migration
1040 of known complexes and proteins.
1041 **Table S4**: Subunit annotations of *Perkinsus marinus* proteins used in this study.
1042 **Table S5**: Complexome profiles of protein complex subunits investigated in this study. Data from both
1043 mitochondrially-enriched samples and whole-cell material. Abundance information is displayed as
1044 normalized relative abundance values.
1045 **Table S6**: Mass spectrometry data from purified ATP synthase.
1046 **Table S7**: Phylogenetic analysis of ATPTG1 proteins.